Photocatalytic CO_2 reduction to C2+ products

*Josep Albero, Yong Peng and Hermenegildo García**

Instituto Universitario de Tecnología Química CSIC-UPV, Universitat Politècnica de València, Avda. De los Naranjos s/n 46022, Valencia, Spain.

KEYWORDS. Photocatalysis, CO_2 reduction, solar fuel, selectivity, C2+ products.

ABSTRACT

There is a considerable interest in the development of photocatalytic CO_2 conversion by sunlight since this process has similarities with natural photosynthesis on which life on Earth is based. At the moment, most of the efforts in this field have been aimed at increasing the productivity, rather than at the control of the product distribution. Particularly, compounds with two or more carbons (C2+) have higher added value than methane, carbon monoxide or formate that are typically the major products of CO_2 reduction. This review focuses on those reports that have described the formation of compounds of two or more carbon atoms (C2+) in the photocatalytic CO_2 reduction either by H_2O or as H_2 as source of electrons and protons. The existing literature has been organized according to the main factor considered as responsible for the selectivity to C2+ products, including photocatalyst structuration, co-catalyst nature, influence of defects, effects of surface plasmon band. Emphasis has been made on remarking the current

empirical knowledge based on experimental results and the lack of predictive capability that could lead to the development of efficient photocatalytic systems for C2+ production.

1. INTRODUCTION

The light-driven conversion of CO_2 and water into chemicals and fuels with the aid of a photocatalyst, mimicking the natural photosynthetic process, is considered among the most promising approaches for decreasing atmospheric CO_2 emissions,[1-7] an action that would contribute to climate change mitigation, while providing renewable fuels. When using solar light and a photocatalyst, this process is generally known as *artificial photosynthesis,*[8-12] since the system and the products are different from those of natural photosynthesis that transforms the same reagents in the leaf chloroplasts to produce O_2 and glucose (**Scheme 1**).

	Artificial photosynthesis	Hydrogenation
Source of e^- and H^+	H_2O	H_2
Typical productivity	$\mu mol \times g^{-1}$	$mmol \times g^{-1}$
Typical temperature	Ambient	>150 ºC

Operation	batch	Possibility of continuous flow

Scheme 1. Specific features of photocatalytic CO_2 reduction either by H_2O or by H_2.

The current solar-to-fuel efficiency of artificial photosynthesis is, however, below or nearby 1 %, and it has to be increased in most of the cases. It has been suggested that an ideal solar-to-fuel efficiency > 10 % is required for artificial photosynthesis to be economically feasible.[13] In addition, the transformation should be performed under continuous flow, before it can be considered as a potentially viable large-scale process.

Chemical reduction of CO_2 by H_2O into useful fuels and chemicals faces a high energy penalty as consequence of the high dissociation energy of the C=O bonds (approximately 750 KJ/mol)[14] and the strength of the O-H bonds. The extremely high endothermicity of the process determines that most of the studied photocatalysts are wide bandgap semiconductors, particularly transition metal oxides (TiO_2, $SrTiO_3$, ZnO, SiC, ZnS etc.),[15] that can provide enough thermodynamic driving-force for CO_2 reduction and H_2O oxidation. **Scheme 2** indicates some typical semiconductors and their redox potential of conduction (CB) and valence (VB) bands in comparison with thermodynamic potentials of some CO_2 reduction reactions.

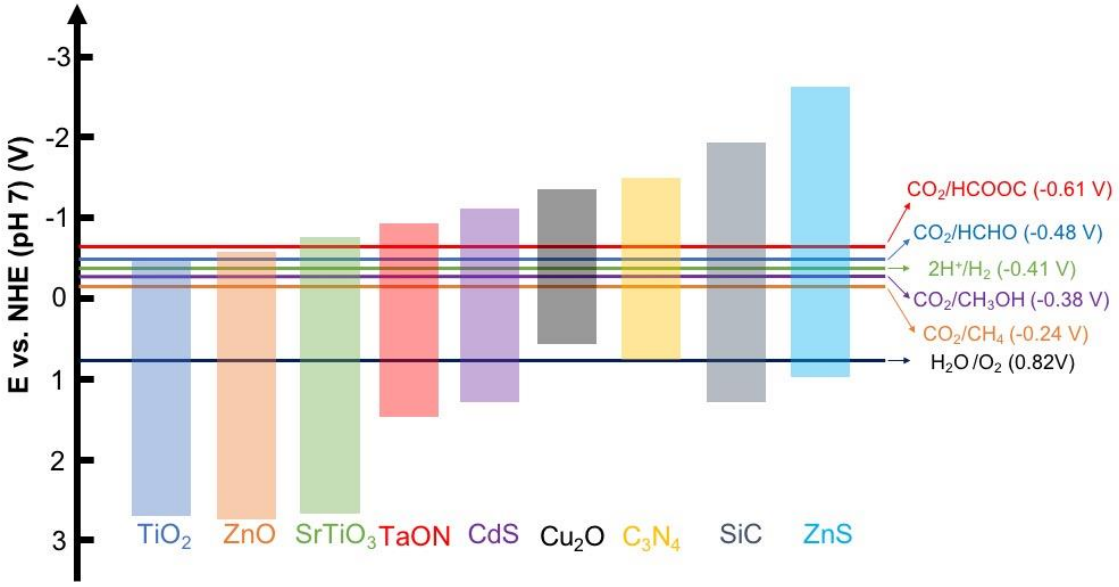

Scheme 2. Conduction and valence band energies of different semiconductor photocatalysts, as well as the electrochemical potentials of some CO_2 reduction reactions to derived compounds and H_2O reduction and oxidation potentials.

The two main limitations faced by the solar-light photocatalytic CO_2 conversion by H_2O as electron source are the low efficiencies of the process and the lack of product selectivity, particularly to high added value chemicals. The main reasons for the low production yields include the use of wide bandgap semiconductors, which typically are able to harvest UV light that corresponds only to about 4 % of the solar spectrum, together with high charge carrier recombination rates. Moreover, common visible light photocatalysts, such as sulfides, selenides, carbides or nitrides, either do not meet the thermodynamic potentials required for simultaneous CO_2 reduction and H_2O oxidation or present serious stability issues under reaction conditions due to photocorrosion in the reaction media.

A way to overcome the low efficiencies currently reached in *artificial photosynthesis* in which H_2O is the reducing agent is to use other alternative electron source with lower oxidation potential than H_2O. Due to its availability and lack of byproducts, an important reducing agent alternative to H_2O is molecular H_2 (Scheme 1). To meet the carbon neutral balance, the stoichiometric H_2 amounts needed to react with CO_2 have to be obtained from renewable sources and not from fossil fuels.

In contrast to the unfavorable thermodynamics of the CO_2 with H_2O reaction, hydrogenation of CO_2 to form various products is an exothermic process, the exact reaction enthalpy depending on the product.[16-21] Equations 1-11 summarizes the redox reactions of commonly reported products from photocatalytic CO_2 reduction, indicating the equillibirum potential and reaction enthalpy. CO_2 hydrogenation is more commonly performed in the dark using thermal catalysis. In spite of being exothermic reactions, the temperatures required for CO_2 hydrogenation are above 250 ºC, typically between 300 and 500 ºC, due to its slow kinetics.

Interestingly, this CO_2 reduction by H_2 can also be promoted photocatalytically with the advantage respect to the thermal process of the possible use of solar light as energy source.[22, 23] Besides, the efficiencies and productivities of the photocatalytic CO_2 hydrogenation are much closer to the values needed to consider its industrial viability. In addition to reports on artificial photosynthesis, the present review also covers those studies on the photocatalytic CO_2 hydrogenation in which the formation of C2+ products have been described.

$CO_2 + 2e^- + 2H^+ \rightarrow HCOOH_{(aq)}$ ($-0.12\ V\ vs.\ RHE$; ΔH^o_R = -31.2(KJ/mol)) (Eq. 1)
$CO_2 + 2e^- + 2H^+ \rightarrow CO_{(g)} + H_2O$ ($-0.10\ V\ vs.\ RHE$; ΔH^o_R = -41.2(KJ/mol)) (Eq. 2))
$CO_2 + 6e^- + 6H^+ \rightarrow CH_3OH_{(aq)} + H_2O$ ($0.03\ V\ vs.\ RHE$; ΔH^o_R = -131.0(KJ/mol)) (Eq. 3))
$CO_2 + 8e^- + 8H^+ \rightarrow CH_{4\,(g)} + 2H_2O$ ($0.17\ V\ vs.\ RHE$; ΔH^o_R = -253.0(KJ/mol)) (Eq. 4))
$2CO_2 + 8e^- + 8H^+ \rightarrow CH_3COOH_{(aq)} + 2H_2O$ ($0.11\ V\ vs.\ RHE$; $\Delta H^o_R = 122.1$(KJ/mol)) (Eq. 5))
$2CO_2 + 10e^- + 10H^+ \rightarrow CH_3CHO_{(aq)} + 3H_2O$ ($0.06\ V\ vs.\ RHE$; $\Delta H^o_R = 130.1$(KJ/mol)) (Eq. 6))
$2CO_2 + 12e^- + 12H^+ \rightarrow C_2H_{4\,(g)} + 4H_2O$ ($0.08\ V\ vs.\ RHE$; $\Delta H^o_R = 127.8$(KJ/mol)) (Eq. 7))
$2CO_2 + 14e^- + 14H^+ \rightarrow C_2H_{6\,(g)} + 4H_2O$ ($0.14\ V\ vs.\ RHE$; $\Delta H^o_R = 264.3$(KJ/mol)) (Eq. 8))
$2CO_2 + 12e^- + 12H^+ \rightarrow C_2H_5OH_{(aq)} + 3H_2O$ ($0.09\ V\ vs.\ RHE$; $\Delta H^o_R = 216.1$(KJ/mol)) (Eq. 9))
$3CO_2 + 20e^- + 20H^+ \rightarrow C_3H_{8(g)} + 6H_2O$ ($0.09\ V\ vs.\ RHE$; $\Delta H^o_R = 374.2$(KJ/mol)) (Eq. 10))
$3CO_2 + 18e^- + 18H^+ \rightarrow C_3H_7OH_{(aq)} + 5H_2O$ ($0.10\ V\ vs.\ RHE$; $\Delta H^o_R = 331.2$(KJ/mol)) (Eq. 11))

2. Aim and scope of the review

With the objective of increasing the process efficiency, the photocatalytic CO_2 reduction has attracted in the last years a growing attention of the scientific community and the number of studies in this area has increased exponentially in the last years. There are in the literature a series of recent reviews covering different aspects of photocatalytic CO_2 conversion, including type of photocatalysts, strategies to increase their efficiency and summarizing the most remarkable achievements reached so far.[24-32]

The present review is focused on those studies on photocatalytic CO_2 reduction reporting the appearance of products with more than one carbon, generically termed as C2+ products. Thus, rather than overlapping with the existing literature the present article complements them by covering an important aspect of photocatalytic CO_2 reduction that at the moment is poorly understood.

The interest on C2+ compared with C1 products rise from their wider use and, therefore, high added value. Table 1 summarizes the most commonly obtained C1 and C2+ products and their related uses.

C2+ product	Most relevant uses	Market price ($/Kg)[33, 34]
Formic acid	The major use of formic acid is as a preservative and antibacterial agent in livestock feed.	0.74
Carbon monoxide	The main industrial application of carbon monoxide is in the Fischer-Tropsch process to obtain liquid hydrocarbon fuels and in the production of methanol.	0.06
Methanol	One of the main applications of methanol is as feedstock in the production of formaldehyde, acetic acid and methyl tert-butyl ether. It is also used to produce hydrocarbons and as gasoline additive. Methane is also a relevant energy carrier since it can store hydrogen and methane and vehicles fuel.	0.58
Methane	As the major constituent of natural gas, its mainly applied as fuel for electricity generation in gas turbine as well as for ovens, homes, water heaters, kilns, automobiles and for domestic heating and cooking. It is also used in industry as chemical feedstock to produce hydrogen.	0.18
Ethane	Mainly used as feedstock in the production of commodity chemicals, mainly ethylene. Also used as refrigerant in cryogenic refrigeration systems.	4
Ethylene	Widely used in the chemical industry for: - Polyethylene production, which is the most widely used plastic and consumes half world's ethylene supply; - Ethylene oxide, used for the production of surfactants, detergents and ethylene glycol; - Ethylbenzene which is precursor of polystyrene; and - Ethylene dichloride, among others.	1.3
Propane	Mainly used as domestic and industrial fuels, as well as in bus and tracks engines. Also used as refrigerator and feedstock.	8
Propylene	Widely used in paint and adhesive industry as feedstock for the production of polypropylene, isopropanol, propylene oxide, acrylonitrile, cumene and acrylic acid, among others.	0.9
Ethanol	It has very different applications such as: antiseptic in medical uses, beverages fabrication, fuel, precursor of feedstocks (ethyl halides, ethyl esters, diethyl ether and ethyl amines), solvent and low temperature liquid to keep vessels a temperatures bellow 0 ^{0}C.	1
Acetic acid	Typically used in the industrial production of monomers such as vinyl acetate, esters (ethyl acetate, n-butyl acetate), food (vinegar) and medical uses.	2.9
Acetaldehyde	Precursor of pyridine derivatives and pentaerythriol to produce resins.	4.45

Methyl formate	Primarily used to manufacture formamide and dimethyl formamide.	4.5

Considering the higher value of C2+ products compared to the C1 analogues, besides the continuous interest in increasing the activity of the photocatalytic CO_2 reduction, some studies have been recently directed towards driving the product selectivity towards C2+ hydrocarbons. The present manuscript summarizes the different approaches that have been developed so far to control product selectivity towards C2+ products, highlighting the most promising strategies. The subject of the present review are those photocatalytic systems that have reported a significant percentage of C2+ products, trying to present the hypothesis about origin is this selectivity. The reader is referred to the existing literature for a comprehensive coverage of the photocatalytic CO_2 reduction.

The emphasis will be done on describing the current state of the art and the reported photocatalysts to form C2+ products from photocatalytic CO_2 reduction, either using H_2O or H_2 as reducing agent. It will be commented that the present knowledge is rather empirical and based on results, there being a lack of theoretical and mechanistic understanding of the factors that control this selectivity. The purpose of this review is to trigger additional research and theoretical models with the long term to design photocatalysts with enhanced selectivity towards C2+ products.

3. Product selectivity

Photocatalytic H_2O splitting can only afford H_2 as product. In contrast, in the case of photocatalytic CO_2 reduction there are a wide range of gaseous and liquid possible products. Moreover, since H_2O can be a reagent in the photocatalytic CO_2 reduction, the occurrence of competitive H_2 evolution can also be observed, frequently as the major reduction product, accompanying other compounds derived from CO_2.

Therefore, besides issues related to photocatalyst activity and stability, previously commented, another important aspect considered of lesser importance in photocatalytic CO_2 reduction, regardless the nature of the electron donor, is product selectivity.

Photocatalytic CO_2 reduction in the gas phase leads generally to CH_4 or CO as major products, while in the liquid phase, formate is the most commonly observed prevalent product. In this regard, although product selectivity has received less attention so far, formation of organic compounds with two or more carbon atoms has been also typically observed, although in much lesser proportions than the major C1 product, generally in combined selectivity values below 5 %. However, techno-economic studies point out that direct conversion of CO_2 to C2+ products, either saturated or unsaturated hydrocarbons or oxygenated products, such as ethane, propane, ethylene, ethanol and propanol, would be much more attractive considering the higher market price per ton of these C2+ compounds compared to the C1 products.[35] The higher added value of C2+ compounds compared to C1 analogues is a driving force to develop selective photocatalytic systems that provide these C2+ products from CO_2 in high yields, but this important consideration of the relative product value has been barely taken into account so far.

Among the reasons for the observed preferential CO_2 reduction to CO, CH_4 or HCOOH, rather than yielding C2+ hydrocarbons or alcohols, the complex kinetic of these reactions, that are

frequently considered as a black box, as well as the lack of catalytic activity towards C-C coupling of the most commonly employed co-catalysts have been pointed out.[36, 37] Thus, typical co-catalysts are transition metals with well-established activity in hydrogenation reactions, rather than in C-C coupling. On the other hand, there is a current gap in the understanding of the rate determining steps in the reaction mechanism that drive selectivity towards C2+ products.

There are nevertheless some common traits for most of the photocatalytic systems in where C2+ products are observed. Since, multiple electron coupled to proton transfer (MECPT) reactions and C-C coupling steps have been identified as the main mechanism for C2+ products formation,[36, 38] it appears that those conditions or systems favoring MECPT also favor the formation of C2+ products. Thus, it turns out that since the e^-/h^+ recombination is a general process limiting the transfer of multiple electrons in a short time and at a given location, this energy waste e^-/h^+ recombination not only decreases the CO_2 conversion, but it also drives product selectivity towards C1. **Scheme 3** shows the energy diagram indicating ideal charge transfer kinetics timescale indicating the stoichiometric number of e^- and H^+. As it can be noted in this Scheme 3, all the reactions leading to C2+ products are characterized by a large number of e^- and H^+ couplings, higher than 8. Thus, in a simple understanding, reaction conditions or materials that favor a large concentration of e^- photogeneration and storage are more favorable for the formation of larger proportions of C2+ products, while other conditions favor the exclusive observation of C1 compounds. These reasons justify why formation of C2+ products is very challenging in comparison to the C1 ones.

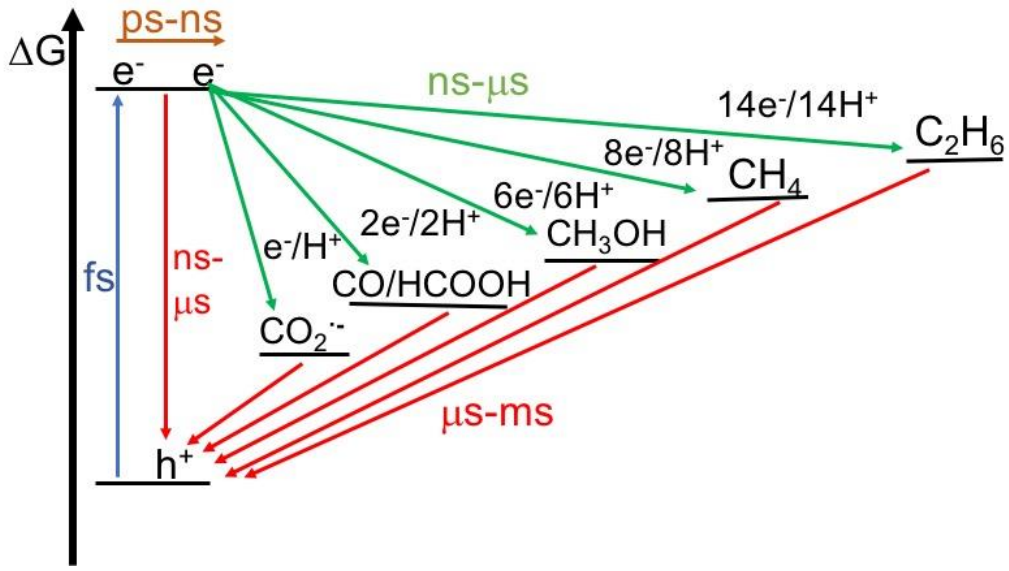

Scheme 3. Energy diagram of the different CO_2 reduction products, indicating the number of e^- and H^+ required and range of the charge transfer reactions timescale, including light absorption (blue), charge migration (orange), charge transfer and reaction kinetics (green), and charge recombination (red).

The scarcity of photoassisted processes generating C2+ hydrocarbons contrasts with conventional Fischer-Tropsch synthesis, where CO and H_2 mixtures are efficiently transformed to liquid fuels or organic oxygenates (i.e. methanol, ethanol and mixed higher alcohols). **Scheme 4** illustrates the differences in the product distribution between photocatalytic CO_2 reduction and Fischer-Trospch synthesis (FTS). However, FTS are usually based upon Fe or Co catalysts and operates under high temperature (310-340 ^oC for Fe and 210-260 ^0C for Co) and pressure (1 – 10 Atm) ranges, which results in very high energy consumption and the associated CO_2 emission due to the water-shift reaction. In addition, conventional FTS presents a carbon efficiency range from 25 to 50 % and a thermal efficiency of about 50%.[39, 40]. In contrast, photocatalytic or photothermal

processes, which energy driving force to carry out the reaction is taken from solar light, would be more convenient.

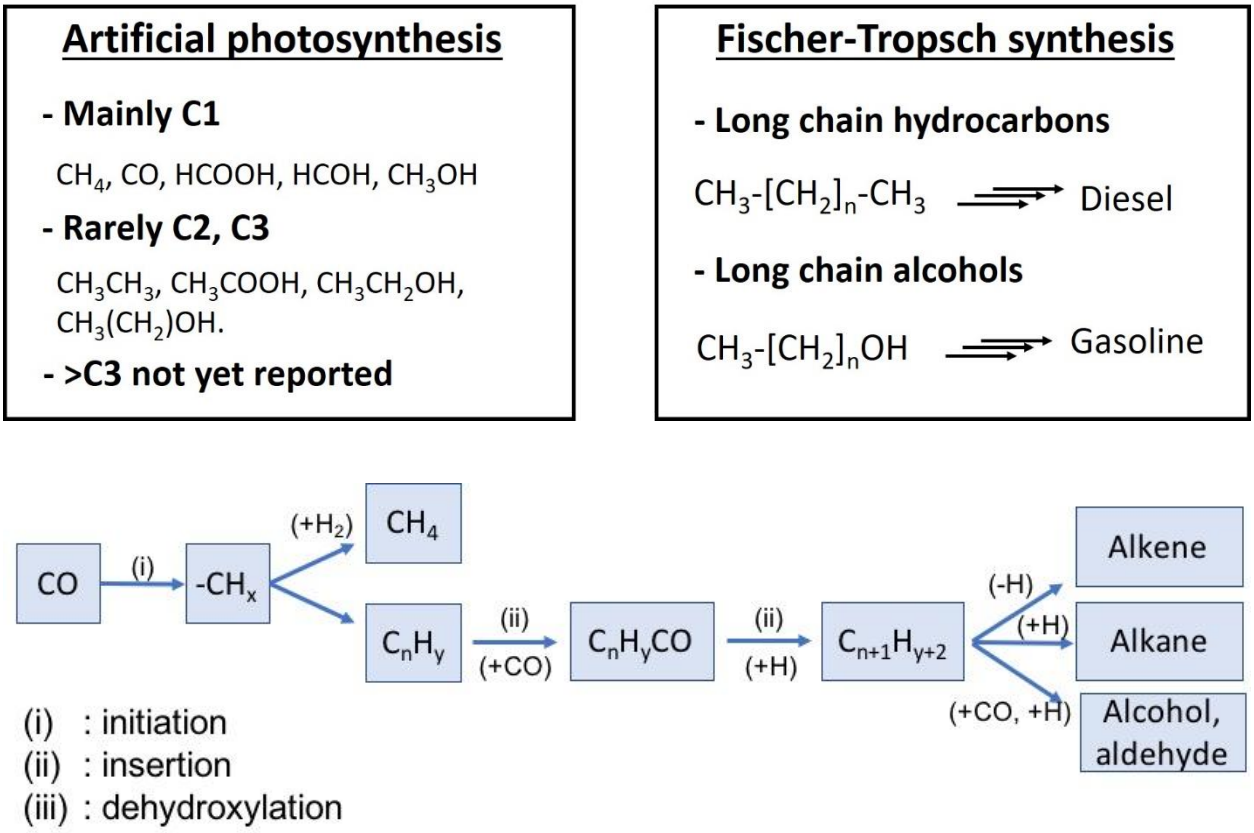

Scheme 4. Typical products on CO_2 reduction by H_2 compared to Fischer-Trospch synthesis (top). Fischer-Tropsch CO insertion chain grown mechanism, indicating the possible selectivity (botton).

The Fischer-Tropsch synthesis follows a polymerization mechanism, where CO undergoes activation on metal (Ru, Ni, Co or Fe) or metal carbide forming adsorbed CH_x and OCH_X (being x= 0-3) intermediates that react by a sequence of consecutive coupling to produce C_nH_m or C_nH_mO products (Scheme 4). Depending on the catalyst, H_2/CO ratio, total pressure, temperature and other

reaction conditions, the primary products can eventually undergo hydrogenation or dehydrogenation to obtain the final paraffin or olefin compounds. In this field, it is widely accepted that Fe is not as efficient as Co or Ru as hydrogenating site, but instead Fe is more selective towards olefins and oxygenated compounds ($\chi \approx 60$ %)[41, 42] On the contrary, Co has been reported to be highly selective for paraffin production.[43-45] Since CO_2 can give rise to CO as primary product, it can be envisioned that analogous Fischer-Tropsch oligomerization could also be possible in CO_2 hydrogenation, although the reaction pathway will be completely different.

In comparison to conventional thermal catalysis, the factors governing the selectivity in photocatalytic CO_2 reduction are still poorly understood. Possible parameters that should influence product selectivity include light intensity, photon energy, photocatalyst properties (crystallinity, defects, etc.) and co-catalyst composition, among others. Understanding of the interplay of all these parameters with the mechanism pathway network is necessary to enhance selectivity towards C2 products. The complexity of the multistep mechanism of CO_2 conversion to hydrocarbons determines a significant kinetic bottleneck compared to simpler reactions such as CO production or even competitive H_2 evolution. Understanding of the reaction mechanism and the parameters influencing product selectivity should lead to the rational design of suitable photocatalytic system that can overcome the kinetic hindrances, reaching the appropriate balance between hydrogenating ability and C-C coupling in the reaction mechanism, resulting in an optimal C2+ product formation.

4. Photocatalysts rational design

One of the most widely explored strategies to enhance the selectivity of the photocatalytic CO_2 reduction towards C2+ products has been photocatalyst architecture engineering. The photocatalytic system is typically constituted by a semiconducting material on which a metal and/or metal oxide co-catalyst has been deposited on its surface. Elemental composition and crystal phase of the semiconductor, preparation and deposition procedures, particle size and location on the semiconductor are typically factors that control the influence of these co-catalysts on the photocatalytic reaction. Due to the opposite nature of e^- and h^+, the complete photocatalytic system may contain two different co-catalysts to manage separately e^- or h^+ transfer.

In one of the first examples reporting the influence of the photocatalyst structure on the formation of C2+ products, Xia and coworkers showed in 2007 the formation of ethanol in the photocatalytic CO_2 reduction.[46] In this study, multi-walled carbon nanotubes (MWCNTs) supported TiO_2 were prepared. Depending on the preparation conditions, the TiO_2 phase and morphology were anatase as NPs or rutile as nanorods (**Scheme 5**). Composites of MWCNT-coated anatase TiO_2 NPs were obtained by sol-gel, while hydrothermal synthesis promoted the formation of rutile TiO_2 nanorods on the MWCNTS. These two composite photocatalysts produced different C_2H_5OH, HCOOH and CH_4 amounts upon UV light irradiation (15 W UV lamp, λ= 365 nm). Thus, the selectivity towards C_2H_5OH (12 e^- + 12 H^+) in anatase NPs/MWCNTs composites was significantly higher (χ= 69.7%), while HCOOH (2 e^- + 2 H^+) was the main product of the irradiation using rutile nanorods/MWCNTs photocatalyst.

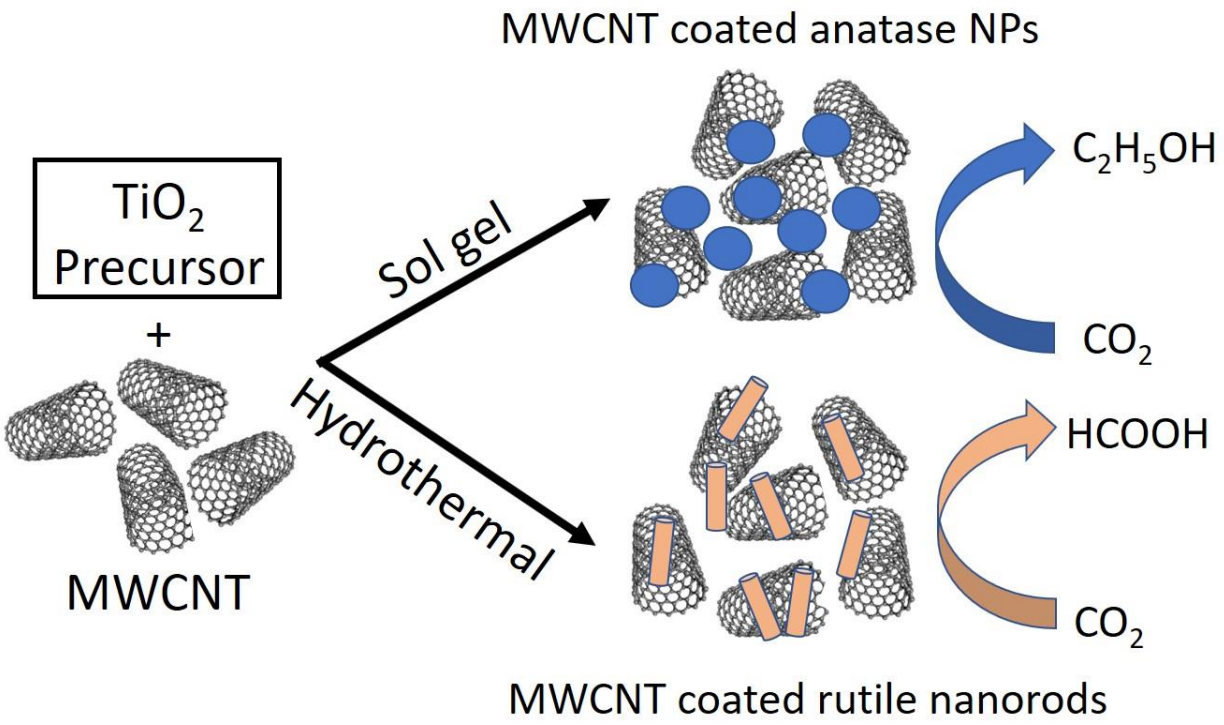

Scheme 5. Preparation and structure of two TiO_2/MWCNTs and their different product selectivity.

The authors ascribed these selectivity differences to the different TiO_2 crystal phase and morphology, although the reason why the two TiO_2 phases exhibit different selectivity still remain to be understood.[46] In this regard, it is worth remarking that the different photocatalytic behavior of TiO_2 crystal phases is well established. For instance, anatase TiO_2 single crystals have been found more suitable for photocatalytic pollutant degradation, while rutile TiO_2 exhibits higher photocatalytic activity towards H_2 evolution.[47] However, even accepting that different semiconductor phases may exhibit different photocatalytic activity, the factors that drive selectivity to ethanol or formic acid still remain unclear.

To gain further understanding on the origin of the product selectivity, a comparison of the catalytic activity of the TiO_2/MWCNT system with those of bare TiO_2 anatase NPs and rutile nanorods was also provided. It was observed that in the case of bare anatase TiO_2 NPs, the three products, C_2H_5OH, HCOOH and CH_4, are also formed in similar proportions in the absence of MWCNTs, although the total production obtained was lower. Conductive carbon nanoforms such as MWCNT and graphenes in appropriate proportion are known to increase the photocatalytic activity of TiO_2 photocatalysts. It is widely accepted that the main reason for this positive influence of carbon nanoforms on the photocatalytic TiO_2 activity derives from their electron conductivity that favors electron delocalization. In line with the general influence of carbon allotropes, in the present case the authors proposed that the e^-/h^+ pairs photogenerated in the TiO_2 are prone to suffer fast recombination. However, the MWCNTs in close contact with the TiO_2 NPs promote efficient charge separation, by migration of CB electrons from TiO_2 to MWCNTs and fast delocalization, therefore, decreasing e^-/h^+ recombination. Delocalization on different components of the charge carriers increases their lifetime and makes more probable their transfer to the reactants. Overall, it appears that the semiconductor crystal phase determines the selectivity, while the MWCNT co-catalyst boosts the production yield.

Importantly, the authors claimed that the good electrical properties of MWCNTs favoring fast e^- transport should also make possible the access of CO_2 to multiple e^-.[46] This is a key point since considering the equations shown in Scheme 3, MECPT has to occur to form ethanol.

In a different example, Lee et al.[48] reported the preparation of Rh-doped Degussa P25 TiO_2 NPs sensitized with the natural light harvesting complex II of green plants (LHCII).[48] **Scheme 6** illustrates the structure of the LHCII/Rh:P25 TiO_2 photocatalyst and the product distribution. LHCII is well-known to absorb photons in the range of 400 – 700 nm, transferring this energy to

the photosystem II reaction center.[49] In the present case, LHCII adsorbed in Rh:TiO_2 NPs gave rise to acetaldehyde (10 e^- + 10 H^+) with selectivity of 78.4%, while CO was the main product (χ= 94.1 %) when bare Rh:TiO_2 NPs were used as photocatalysts. Methyl formate (8 e^- + 8 H^+) was also detected in both cases, although in lesser extend (χ= 5.9 %). The authors ascribed the selectivity towards CH_3CHO to the visible light photosensitization of LHCII to the Rh:TiO_2 NPs. Although the authors did not addressed whether an energy or charge transfer mechanism was responsible of the enhanced selectivity,[48] it seems clear that visible light photogenerated charges in LHCII contributed not only to enhance the photocatalyst activity, but also to determine the selectivity towards C2+ products probably due to the larger charge density available. It is worth noticing that the photocatalytic tests were carried out at high photon flux (362 mW/cm^2), thus favoring a large photo-induced charge density generation.

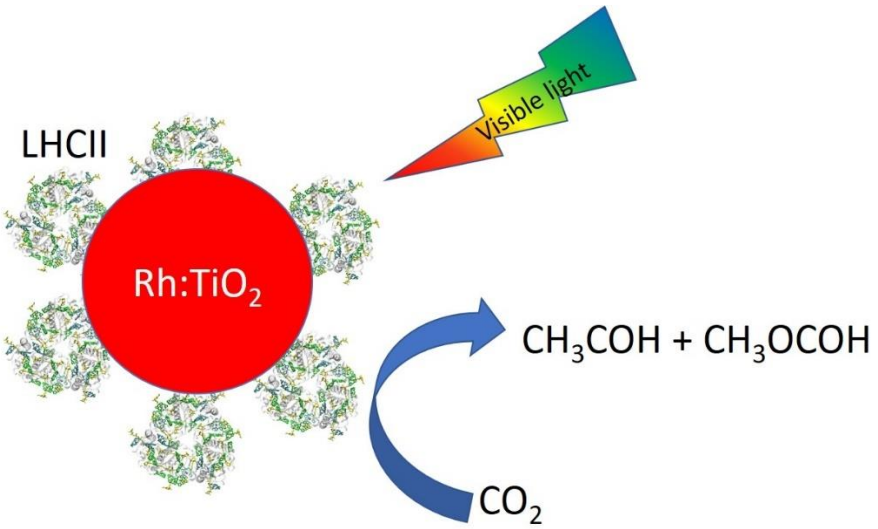

Scheme 6. Structure and product selectivity of LHCII/Rh:P25 TiO_2 photocatalyst.

Although TiO_2 in various forms is the most widely studied photocatalyst, other semiconductors can also promote light-induced CO_2 reduction forming C2+ products. In this

regard, Shown et al.[50] reported the preparation of graphene oxide (GO) supported Cu NPs for photocatalytic CO_2 reduction (**Scheme 7**). In this example, Cu NPs were strongly grafted to the GO surface using a microwave-based preparation method. GO is known to generate e^-/h^+ pairs upon light absorption and Cu NPs were used as electron reservoirs, reducing the recombination rate and enhancing the MECPT. The addition of 5 wt% Cu in GO promoted methanol ($6\ e^- + 6\ H^+$) and acetaldehyde ($10\ e^- + 10\ H^+$) production in similar proportions as main products, while H_2 was detected in a minor extend, upon UV-Vis light irradiation (Halogen lamp; 100 mW/cm^2). Cu content increase (10 wt%) improved the photocatalytic activity, although similar selectivity was obtained. However, further increase up to 15 wt% Cu shifted the selectivity, being χ= 54% and 45% for CH_3CHO and CH_3OH, respectively. The authors have explained the selectivity shift as a function of the Cu loading as being a consequence of GO CB and VB shift due to the strong Cu-GO grafting. XPS analysis of the samples showed that the increase in Cu content promoted a proportional decrease in the concentration of -COOH and C-O-C functional groups characteristic of GO, thus modifying its electronic properties and reducing its work function. UPS measurements combined with diffuse reflectance UV-Vis absorption spectroscopy of the samples allowed determination of CB and VB for each photocatalysts (**Scheme 7**).

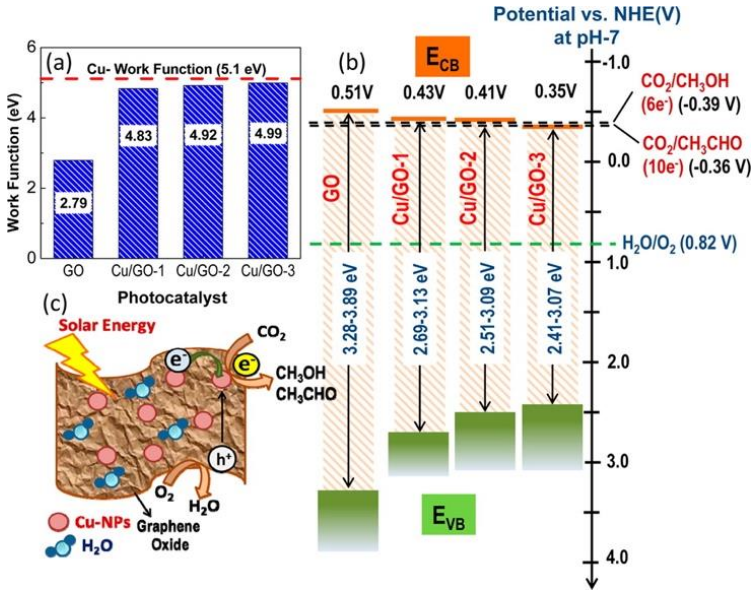

Scheme 7. GO band gap and Cu work function (a), band edge positions of GO and GO/Cu composites with different Cu content and the CH_3OH and CH_3CHO potential (b) and schematic illustration of the reaction mechanism (c). Reproduced with permission.[50] Copyright (2014) American Chemical Society.

The variation of product selectivity in Cu-GO was justified based on thermodynamic potentials. The calculated CB energy for samples containing 5 and 10 wt% of Cu clearly shows the feasibility of the multi electron reduction of CO_2 to methanol and acetaldehyde. However, the CB position of the photocatalyst containing 15 wt% of Cu is apparently lower than the CO_2/CH_3OH reduction potential, but still higher than that of CO_2/CH_3CHO, therefore, leading to preferential acetaldehyde production.[50] At this point it should be commented that thermodynamic potentials never indicate the activation energy barriers of the reactions and that in general thermodynamics are more favorable as the number of e- and H+ added to CO_2 increases, but a large number of MECPT steps is also unfavorable from the kinetic point of view. In other words,

there are surely other possible products with more favorable thermodynamics than acetaldehyde, but they are not being detected in the photocatalytic reaction.

In a related example of the photocatalytic CO_2 reduction by H_2O by Cu_2O NPs with preferred 200 facet orientation strongly grafted on few-layers defective graphene, formation of H_2 χ= 80%) and CH_3CH_2OH (12 e^- + 12 H^+) with an estimated production rate of 545 μmol g^{-1} h^{-1} (χ= 20%) was also observed.[12] **Scheme 8** illustrates the photocatalytic system and the products formed. Due to the ability of graphene to coat glass surface, the defective graphene-based photocatalyst was immobilized inside a capillary reactor, while the system was irradiated at 254 nm (28.3 mW/cm^2) and operated under liquid-phase continuous flow with a Taylor flow regime. The Taylor flow regime in capillaries alternate visually observable liquid and bubbles in the flow. Generation of H_2 in about four-fold higher rates than CO_2 reduction was also observed. No reasons for the apparent exclusive formation of ethanol in this photocatalytic process were given and it would be important to revisit this photocatalytic system, particularly considering that it is one case of continuous flow reaction.

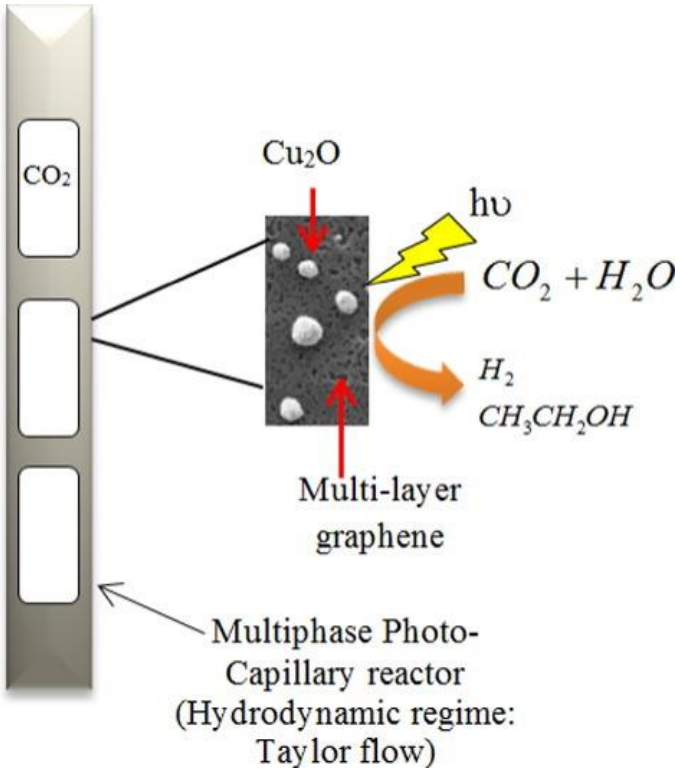

Scheme 8. Structure of the photocatalytic system comprising oriented Cu_2O NPs grafted on defective graphene and the observed product distribution. Reproduced with permission.[12] Copyright (2016) Elsevier.

In a different approach, porous single crystal (PSC) TaON microspheres have demonstrated photocatalytic activity towards ethanol (12 e^- + 12 H^+) and ethanal (10 e^- + 10 H^+) production as only products under visible light irradiation (1002 W/m^2, λ > 420 nm) (**Scheme 9**).[51] Materials with PSC structure have shown higher photocatalytic activity due to the lack of surface boundaries within the single crystal, thus reducing recombination events, and the presence of porosity that increases the adsorption sites of substrates.[16] The selectivity towards CH_3CH_2OH and CH_3CHO was of 83.3% and 16.7%, respectively. Interestingly, the addition of Pt NPs (0.5 wt%) to the TaON

PSC microspheres improved the ethanol selectivity (χ= 89.5 %), while the total solar to hydrocarbon efficiency remained unchanged. The authors propose that the Pt NPs act as e^- sinker, boosting the photoinduced charge separation efficiency. The enhanced number of charges concentrated at these Pt NPs would contribute to further reduce the generated ethanal to ethanol, resulting in an improved reaction selectivity, instead of an increase of the overall photocatalytic activity.[51]

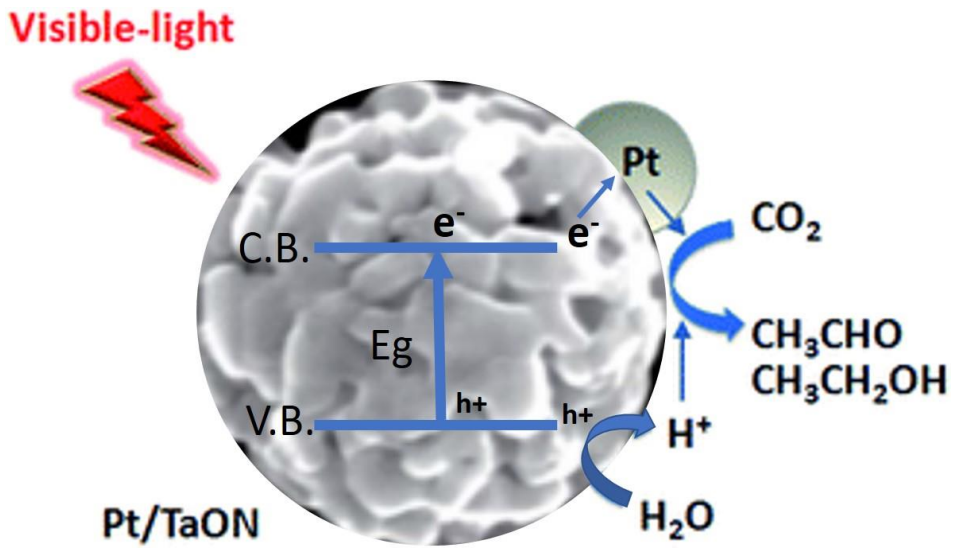

Scheme 9. Structure of PSC TaON doped with Pt and products observed on the photocatalytic CO_2 reduction. Reproduced with permission.[51] Copyright (2016) Royal Society of Chemistry

Overall, selection of a suitable photocatalyst/co-catalyst combination has been found frequently crucial for the increase of the selectivity towards C2+ products. The semiconductor crystal phase was determined to play a key role on product selectivity. Changes in the crystal phase should lead to small differences in the band energy positions due to differences in the atomic

coordination and geometries of the different atomic planes that should result in differences in the electronic states as well as differences in their intrinsic e^-/h^+ recombination kinetics.

On the other hand, convenient co-catalyst selection has been found crucial not only to enhance the production yield, but also to gain control on the selectivity. Moreover, it has been shown that the interaction semiconductor-co-catalysts can drive the selectivity through fine tuning of the semiconductor optoelectronic properties, as well as to increase the charge density and charge transfer rate. Thus, the co-catalyst properties can be varied by increasing the photogenerated charge density, shifting the semiconductor CB to fine tune its reduction potential or acting as charge carrier reservoir enhancing photocatalyst charge transfer efficiency and reducing the recombination rate. It is the interplay of all these factors, charge separation enhancements and charge recombination dismiss, what can lead to changes in the product selectivity. It is worth commenting that in most of the previous examples UV light has been used as driving force. Therefore, photon energy could play a key role in the photocatalytic C2+ products production, besides high photon flux.

5. Co-catalysts engineering.

Co-catalysts can play various roles in a photocatalytic reaction.[52] One of the better understood roles is to enhance charge separation on the semiconductor by acting as sinkers of photogenerated e^- or h^+. The fraction of e^- or h^+ that reach the co-catalyst exhibits a much longer lifetime, typically in the microsecond time regime or longer. A simple way to provide evidence for this role is to compare by time-resolved absorption spectroscopy the temporal profile of the transient signal

corresponding to the charge separated state of the semiconductor in the absence and presence of the co-catalyst.

Since photogenerated e^- and h^+ accumulate on the NPs of the co-catalysts, it is on these co-catalyst NPs where interaction with the substrates leading to products occurs. Thus, a second role of co-catalysts includes the efficient transfer of the charge carriers to the substrates, particularly CO_2 in this case. Formation of reaction intermediates and primary products should take place preferentially on these co-catalyst NPs, although they can latter migrate to the semiconductor or to the reaction medium. Therefore, not surprisingly, the co-catalysts do also frequently exhibit catalytic activity in reduction and oxidation reactions, besides the positive effect in photocatalysis.

As commented at the end of the previous section, the co-catalyst interaction with the semiconductor can significantly alter the final selectivity of the photocatalytic system. In this regard, the co-catalyst architecture can be the main factor determining a major role in the photocatalytic production of C2+ hydrocarbons.

Among the different approaches to modulate the co-catalyst properties, the use of bimetallic alloys or, alternatively, the incorporation of more than one co-catalyst are two of the most widely used. The rationale behind this approach is to implement the photocatalytic system with co-catalysts of different activity, combining their properties synergistically. For instance, in photocatalytic water splitting, metal NPs (Pt, Au, etc.) and metal oxides (RuO_2, IrO_2, etc.) NPs can be simultaneously present on the semiconducting material in order to favor the H^+ reduction and H_2O oxidation semi-reactions, respectively (**Scheme 10**).[53] Thus, the two co-catalysts play complementary catalytic roles. One of them promotes reduction, they being typically a reduced

transition metal, and second one facilitates oxidation, these being generally an oxidized transition metal, the combination of the two resulting in the overall reaction stoichiometry.

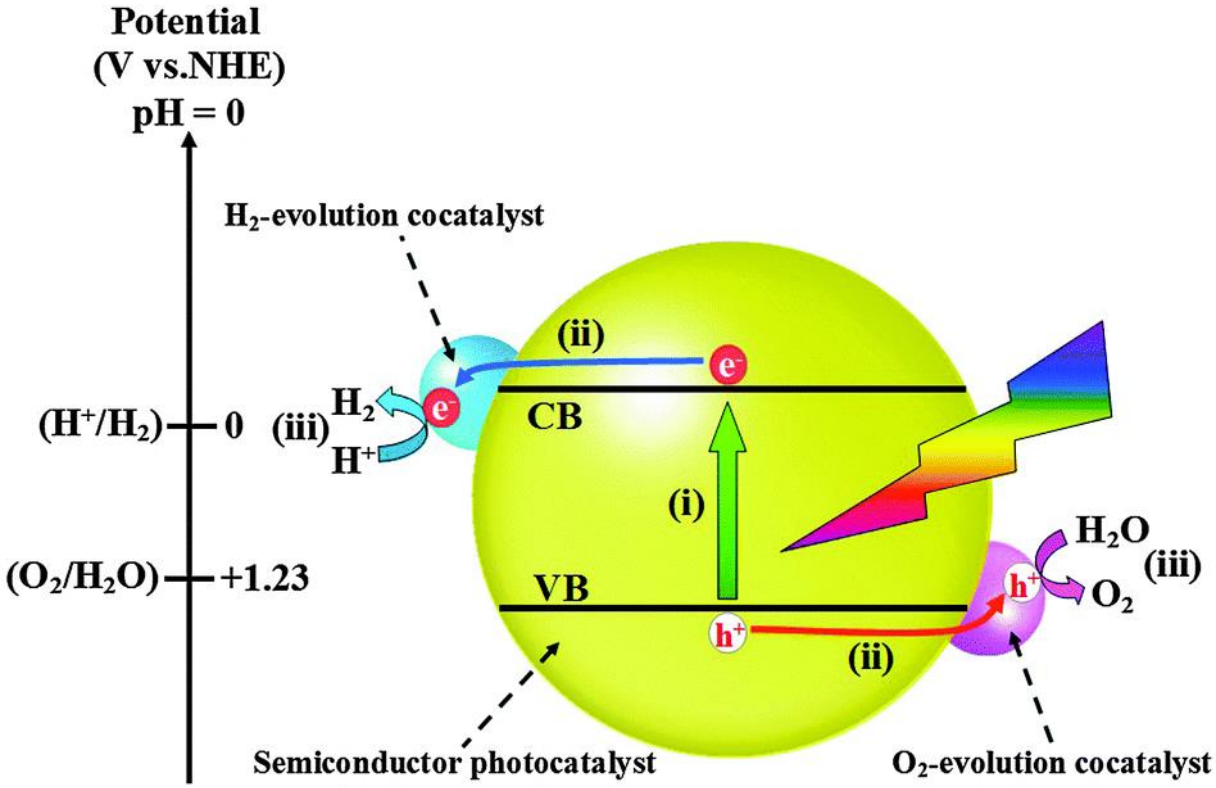

Scheme 10. Illustration of the role of two different co-catalysts deposited on a semiconductor to promote independently the reduction and oxidation semireactions. Reproduced with permission.[53] Copyright (2016) Royal Society of Chemistry.

Analogously to the photocatalytic overall water splitting, two co-catalysts to promote each semireaction have been similarly deposited simultaneously on the semiconductor surface to promote the photocatalytic CO_2 reduction. In the particular case of CO_2 reduction, other desirable properties of co-catalysts are CO_2 adsorption and proton conduction.

For instance, Varghese et al.[54] reported in 2009 a photocatalytic system for CO_2 reduction comprising nitrogen-doped TiO_2 nanotube arrays decorated with equivalent amounts of Pt and Cu NPs deposited by sputtering. N-doping introduces visible light photoresponse on the TiO_2 nanotube array that, otherwise will be active only under UV irradiation. In this work, the author's hypothesis was that Pt NPs are very efficient to promote water reduction to H_2, while Cu NPs, which are known to have high CO_2 adsorption capacity, would be more active in reducing CO_2 to CO. Subsequently, the CO adsorbed on the Cu NPs would react with the atomic hydrogen generated in the Pt NPs to form hydrocarbons (**Scheme 11**).[54] Accordingly, the photocatalytic CO_2 reduction using Pt-Cu NPs supported on N-doped TiO_2 nanotubes produced methane as the main product, together with a mix of olefins, branched paraffins and other alkanes, although in much lower proportions.

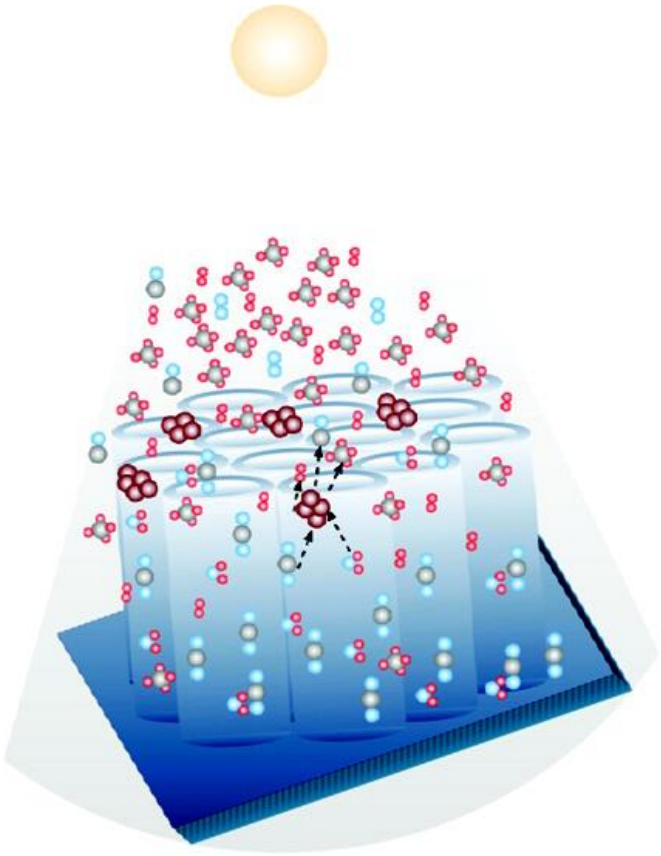

Scheme 11. Illustration of the photocatalysts composed by N-doped TiO_2 nanotubes array containing Pt and Cu NPs in equivalent amounts. Reproduced with permission.[54] Copyright (2009) American Chemical Society.

Importantly, using independent metal NPs, a change in the main product from H_2 to CO was observed for Pt vs. Cu NPs, respectively. There are several examples in the literature reporting also the different selectivity of Cu NPs compared to Pt and Au NPs as co-catalysts, changing the selectivity from H_2 to CO_2 reduction products.[17-19] In the present case or N-doped TiO_2 nanotube arrays, the combined action of Pt and Cu NPs was found to favor the formation of C2+ products, reaching a production rate of 160 $\mu L \times g^{-1} \times h^{-1}$. Optimization of the area of the N-doped TiO_2 nanotube array film covered by Pt and Cu NPs or even formation of alloy of the two metals could have increased further the C2+ production rate.[54]

Similarly to the previous study, Zang et al have increased the selectivity towards C2+ products in the photocatalytic CO_2 reduction by appropriate co-catalyst selection and structuration. These authors[55] reported in 2012 the use of Pt-Cu alloys supported on TiO_2 nanotubes as photocatalysts for CO_2 reduction. In their study, coaxial Pt-Cu alloy shells were grown on a periodically modulated double-walled TiO_2 nanotube array core (**Scheme 12**). Methane (8 e^- + 8 H^+) (χ= 71.4 %), ethane (14 e^- + 14 H^+) (χ= 14.3 %) and ethylene (12 e^- + 12 H^+) (χ= 7.1 %), were obtained when the Cu:Pt atomic ratio was adjusted to 1:2 upon 100 mW/cm^2 irradiation. On the contrary, other Cu:Pt proportions as well as photocatalysts containing only Pt or Cu led to relatively low C2+ hydrocarbon production, being CH4 the main product. Therefore, it is worth noticing that the use of this bimetallic alloy, in the appropriate proportions, was able to shift the

selectivity towards C2+ hydrocarbon. In a simplistic idea, it seems that Pt increases the reduction rates of the photocatalytic process, while Cu gives the selectivity to C2+ products due to the stronger CO adsorption and reactivity on this metal.

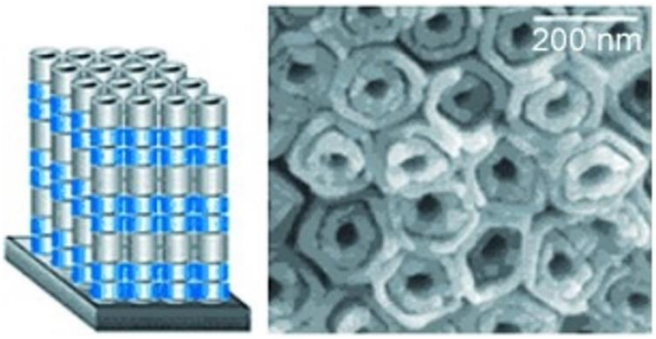

Scheme 12. Structure of Pt:Cu NPs supported on TiO_2 nanotubes and products observed on the photocatalytic CO_2 reduction. Reproduced with permission.[55] Copyright (2012) John Wiley and Sons.

Most of the previous studies refer to the so-called *artificial photosynthesis* in which electrons and protons to reduce CO_2 come from H_2O, similarly to the natural photosynthesis process. However, as mentioned earlier, the current state of the art of artificial photosynthesis is far from any practical application due to the low efficiency and productivity. A less ambitious approach, but deemed more feasible, is the photocatalytic CO_2 reduction by H_2. Depending on the conditions, this photocatalytic CO_2 reduction by H_2 can reach under sunlight irradiation a productivity tens of millimols of converted CO_2 per gram of catalyst per hour. This makes the photocatalytic CO_2 reduction much closer to a viable industrial process, provided that H_2 is obtained from renewable energy sources. As a matter of fact, the catalytic reaction of CO_2 and H_2

can be also promoted thermally in the absence of light,[20, 21] but the use of solar light as primary energy is also appealing.[22]

Following this research line, T. Zhang and coworkers[56] reported recently the photothermal CO_2 hydrogenation over alumina-supported CoFe alloys. The term photothermal alludes to a reaction mechanism based on the conversion of the photon energy on local (nanometric) heat on the NP. Thus, irradiation can cause an abrupt increase of the temperature on the NP surface. This local would not correspond to the macroscopic temperature measured in the bulk system that is an average in where the contribution of the temperature of the NPs can be very minor due to its small proportion. This high local temperature on the NPs can trigger thermal catalytic reaction, particularly considering that NPs are frequently also excellent conventional catalysts. The term photothermal for this type of photocatalytic process indicates the very special and unique way to provide localized heating on the NP by using light and an absorber.

In their study, the CoFe alloys on alumina were prepared by thermal reduction of CoFeAl layered double hydroxide (LDH) nanosheets in H_2 atmosphere at different temperatures (**Scheme 13**). A marked influence of the reduction temperature of the trimetallic LDH on the product selectivity for the photothermal hydrogenation was observed. The selection of the LDH composition was based on the known activity of Fe as an active catalyst for CO_2 conversion to CO, while Co-based catalysts are well-known for C-C coupling in the Fischer-Tropsch process. In this way, it was assumed that Fe should form CO. Subsequently Co should convert this generated CO into C2+ products. Therefore, a synergy between the two metals was expected for light-assisted C2+ hydrocarbons production. The authors reported that LDH thermal reduction at

temperatures below 550 ºC promotes the discrete FeO_x and CoO_x NPs formation on amorphous Al_2O_3, while higher temperatures resulted in the formation alumina supported CoFe alloys. Interestingly, the product selectivity was progressively shifted from CO, when the catalyst was obtained at reduction temperatures between 300 and 400 ºC, to CH_4 when the LDH precursor was treated in the 450 – 550 ºC temperature range, and finally to C2+ products for photocatalysts prepared at temperatures higher than 600 ºC upon 300 W Xe lamp irradiation. Thus, a 35 % selectivity of C2+ products was obtained when alumina supported CoFe alloys, prepared at 650 ºC, were used. Therefore, the product selectivity was easily manipulated through temperature tuning in the preparation of CoFe alloys starting from CoFeAl LDH.[56] (Scheme 13)

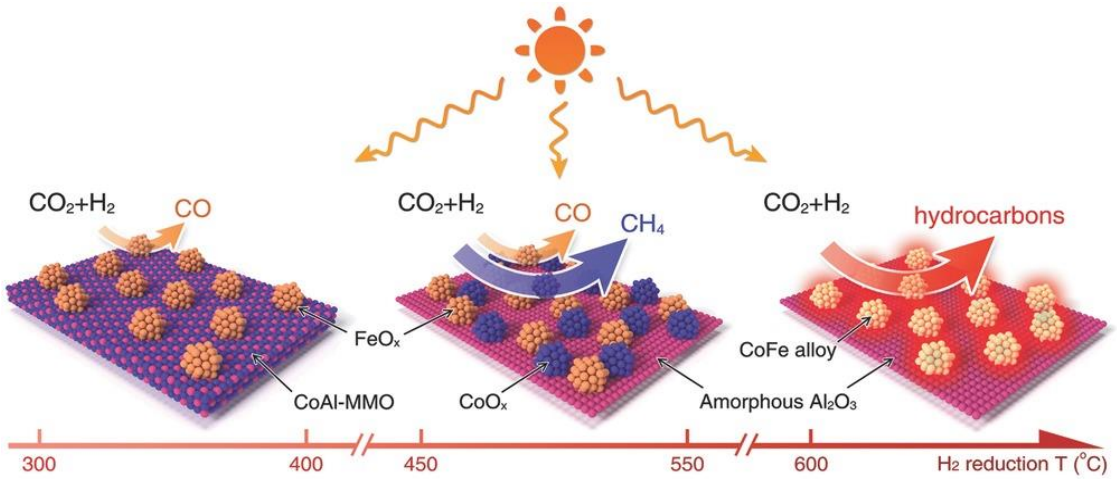

Scheme 13. Illustration of the influence of reduction temperature of the CoFeAl LDH on the product selectivity depending on the formation of different active sites. MMO refers to mixed metal oxide.[56] Copyright (2018) John Wiley and Sons.

Theoretical calculations were carried out in order to unravel the mechanism governing the photocatalytic activity of alumina supported CoFe alloys compared to FeO_x and CoO_x NPs. It was demonstrated that FeO_x species, formed in the LDH treatment at lower temperatures, favor thermodynamically the production of CO. However, CoO_x species, only appearing at medium temperatures, are more prone to favor CO hydrogenation to CH_4, explaining the selectivity shift when the CoFeAl LDH is treated at reduction temperatures between 450 and 550 ºC. Finally, the calculations provided strong evidence that CoFe alloys, formed at the higher temperatures, promote very efficiently C-C coupling reactions, computed as adsorbed CH species reacting with adsorbed CH_2 on the $Co_{11}Fe_5$ (110) surface,[56] thus providing an understanding of the observed selectivity towards C2+ products for the CoFe alloy. This type of calculations on models are very useful in providing understanding on the reaction mechanism and can serve to develop suitable photocatalysts to obtain C2+ based on theory principles.

It is worth noticing that the strategy to use two or more different co-catalysts is not limited to metal NPs. In this regard, Kim et al.[57] reported in 2012 the deposition of a thin Nafion (perfluorinated polymer with sulfonate groups) overlayer on TiO_2 supported Pd NPs as a very convenient method to reduce photocatalytically CO_2 to methane (8 e^- + 8 H^+) , ethane (14 e^- + 14 H^+) (**Scheme 14**). In the absence of the Nafion coating, Pd-TiO_2 photocatalysts showed 95.5 % and 4.5 % selectivity towards CH_4 and C_2H_6, respectively. However, the Nafion overlayer on the Pd-TiO_2 enhanced the C_2H_6 selectivity up to 6.4 % under 300 W Xe lamp irradiation (λ > 300nm).

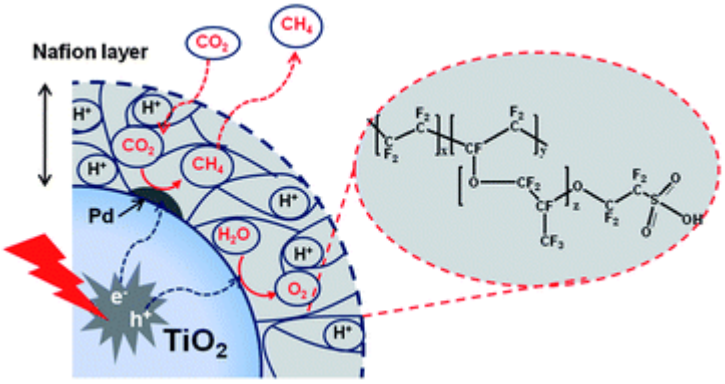

Scheme 14. Structure and photocatalytic activity in CO_2 reduction on Nafion/Pd-TiO_2. Reproduced with permission.[57] Copyright (2012) Royal Society of Chemistry.

The authors pointed out that Nafion main role was the improvement of the proton conduction, facilitating the MECPT steps near the TiO_2 surface. Moreover, CO_2 intermediates could be stabilized in the Nafion layer, which would help to MECPT steps from intermediates to the final product. On the other hand, the Pd NP role was to act as e^- buffer from the TiO_2 CB and subsequently reduce protons. Compared to Pt, Pd has been reported to slow hydrogen atom recombination, diminishing the unwanted H_2 evolution and favoring the CO_2 hydrogenation.[57] Methane was the main product measured using Pd-TiO_2 as photocatalysts. In comparison, ethane production in similar proportion as that of methane, accompanied by small propane amounts, were measured when the Nafion overlayer was deposited on the photocatalyst. Therefore, the use of the Nafion shell to enhance the proton transfer and intermediate stabilization clearly improved the photocatalytic activity towards C2+ products in this photocatalytic system. As a general comment, the extent in which H^+ availability limits the reaction rate of the photocatalytic CO_2 reduction has been insufficiently addressed. It can be expected that also other H^+-conducting membranes or

materials would act similarly on the photocatalytic CO_2 reduction enhancing the proportion of C2+ products and it would be worth to test this hypothesis.

In a different approach, Park and coworkers[58] reported the preparation of sodium trititanate nanotubes (TNTs; $Na_xH_{2-x}Ti_3O_7$) decorated with Cu NPs and overcoated with CdS quantum dots (QDs) (CdS/Cu-TNTs) (**Scheme 15**). This photocatalyst was active under visible light from a 450 W Xe lamp ($\lambda > 420$ nm) irradiation to promote the photocatalytic reduction of CO_2 by H_2O, obtaining CH_4 (8 e^- + 8 H^+) (χ= 49.1 %), C_2H_6 (14 e^- + 14 H^+) (χ= 31.3 %), C_3H_8 (20 e^- + 20 H^+) (χ= 17.9 %), together with C_2H_4 (12 e^- + 12 H^+) and C_3H_6 (18 e^- + 18 H^+) in lesser amounts (0.5 % and 1.3 %, respectively). Interestingly, CO and H_2 were no detected as reaction products. In this multicomponent photocatalytic system, all the elements work synergistically towards hydrocarbon formation. TNT role is to act as basic support, in order to improve the CO_2 adsorption, as well as semiconductor receiving electrons in its CB from CdS and subsequently transferring these electrons to Cu NPs. CdS QDs are not only working as visible light harvesters and TNT photosensitizer, but also it was claimed that stabilizes the initially reduced species ($CO_2^{\cdot-}$). The concentration of Na^+ intercalated in the TNTs plays also a fundamental role in the formation of surface-bound formates from the CdS-stabilized $CO_2^{\cdot-}$. Finally, Cu NPs are the key component for the selectivity shift towards C2+ hydrocarbons, since control experiments in the absence of Cu NPs demonstrated negligible formation of C2+ products. According to this mechanistic proposal, formate intermediates formed near the Cu NPs surface would undergo subsequent reduction yielding C, CH, CH_2 and CH_3 species, which should remain trapped on the Cu NP surface, evolving eventually to C2+ products. Scheme 15 shows the reaction mechanism.[58]

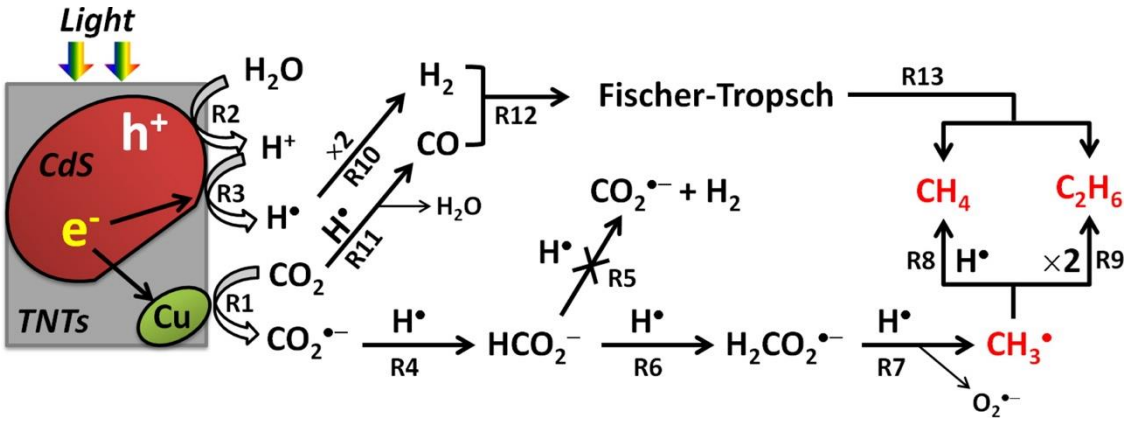

Scheme 15. Proposed mechanism for photocatalytic CO_2 reduction using CdS/Cu-TNTs. Reproduced with permission.[58] Copyright (2015) American Chemical Society.

Catalysts containing alkali metal dopants have been widely reported to enhance CO_2 reduction at high temperatures as consequence of structural and electronic effects induced in the catalysts core structure.[59, 60] The effect of alkali metal dopands is often attributed to a diminution of the work function of the catalysts.[61] The role of Na^+ for the production of C2+ products in photo-assisted CO_2 reduction was also investigated recently by Corma and Garcia in detail.[62] In this study Na^+-promoted Co NPs coated by thin carbon layers (Na-Co@C) were used as photocatalysts in the light-assisted CO_2 hydrogenation upon UV-Vis light excitation with a 1000 W Xe lamp (24KW/m^2) (**Scheme 16**). The major reaction product was CH_4 (χ= 50.2 %), but accompanied by C2+ hydrocarbons in a remarkable 39.5 % selectivity (C2= 13 %, C3= 12.7 %, C4= 5.2 %, C5= 3.3 %, C6 = 2 % and others 3.3%) and 6.5 % selectivity for ethanol (12 e^- + 12 H^+). On the contrary, in the absence of Na^+, CH_4 was formed with almost complete selectivity (> 96 %), thus proving experimentally the promotional effect of Na^+ in this photocatalytic CO_2 reduction.

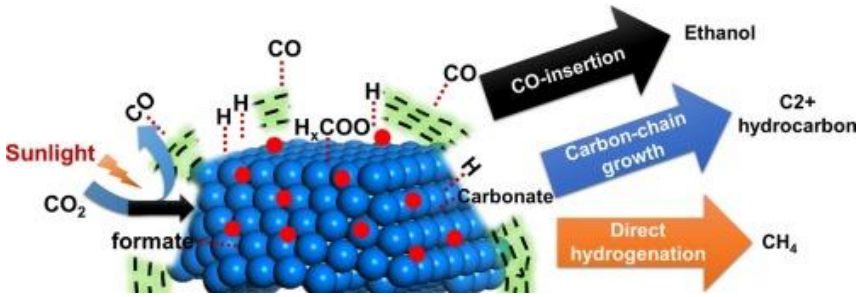

Scheme 16. Structure and photocatalytic activity of Na-Co@C photocatalyst. Reproduced with permission.[62] Copyright (2018) Elsevier.

In order to gain information about the role of Na^+, the surface of the catalyst was monitored by near ambient-pressure XPS. Analysis of the differences in the deconvolution of the C1s peaks provided evidence in support of different reaction intermediates, depending on the presence or absence of Na^+ in the photocatalyst. Specifically, the presence of H_xCOH was detected only in the absence of Na^+. H_xCOH is unstable on the Co surface, leading CH_x formation, which eventually can be hydrogenated to CH_4, explaining the higher selectivity towards CH_4 in the absence of Na^+.

Interestingly, light irradiation also influenced the product selectivity in Na-Co@C, and thus, in the absence of light, under equivalent thermal reaction conditions at 235 ºC, CH_4 was the main product detected. Near ambient-pressure XPS analysis showed that light irradiation affects the formation and stabilization of CO, formate and H_xCOO* intermediates either on Co surface or on the carbon layer.[62] However, under thermal conditions CO could not be detected on those surfaces, but instead only in the gas phase. Thus, light irradiation played an important role in the CO_2 activation to $CO_2^{\cdot-}$ through formation of e^-/h^+ pairs, enhancing the CO_2 dissociation to CO and its stabilization on the photocatalyst surface. It was proposed that CO stabilization contributes to a higher selectivity towards ethanol and C2+ hydrocarbons by a CO insertion mechanism.[62]

Since the factors that promote C-C coupling in the photocatalytic CO_2 reduction are unclear, it appears necessary to shed light in the process by combining experimental detection of the species involved in the process and theoretical calculations, there being at the moment a paucity of studies combining these tools to understand the outcome of the photocatalytic CO_2 reduction.

6. Role of surface defects on CO_2 adsorption and C2+ formation

The generation of surface defects in the way of oxygen vacancies (V_O), interstitial defects or mid-gap states have been widely reported to enhance the photo-catalytic activity in different application.[63-65] Among them, photocatalytic CO_2 reduction is known to be hampered by kinetically challenging MPCET reactions. The introduction of V_o, interstitial defects or mid-gap states that could act as buffers of abundant localized electrons has been proposed to play a positive role in the photocatalytic CO_2 reduction by providing sites concentrating e^- that should assist to overcome MPCET bottlenecks.[66]

Following this assumption, Durrant and In reported methane (8 e^- + 8 H^+) and ethane (14 e^- + 14 H^+) production using Pt-sensitized graphene-wrapped defect-induced TiO_2 photocatalysts upon sun-simulated light irradiation.[67] In this example, Degussa P25 TiO_2 NPs were reduced in the presence of sodium borohydride at 350 ºC in Ar atmosphere, obtaining defect-induced TiO_2. The authors proposed that defects consisting in mid-gap states (Ti $^{3+}$) were generated in the P25 NPs as consequence of the chemical reduction. Then, defect-induced TiO_2 and GO were mixed and annealed in a vacuum oven at 230 ºC. Finally, Pt NPs were photodeposited from H_2PtCl_6 aqueous solution in the presence of MeOH as sacrificial agent. The authors suggested that the synergistic effect between the surface-Ti^{3+} sites and the wrapped graphene is responsible for the ethane

formation. More specifically, ultraviolet photoelectron spectroscopy (UPS) and transient absorption spectroscopy (TAS) studies provided experimental evidence for the occurrence of an efficient charge transfer at the titania/graphene interphase. According to the author interpretation of the TAS data, photogenerated e^- accumulated in the Ti^{3+} sites, reacting with adsorbed CO_2, while holes migrate to graphene promoting proton generation. Theoretical calculations have shown that Ti^{3+} and V_O sites enhance CO_2 adsorption on TiO_2 surface[68, 69] and e^- accumulation can promote CO_2 activation.[70] On the other hand, it is also well-stablished that $\cdot CH_3$ radicals, generated by MPCET in photocatalytic CO_2 reduction[37, 71], can be stabilized by graphene.[72] Therefore, graphene is proposed to act as hole scavenger for a sustained proton supply, but also stabilizing $\cdot CH_3$ radicals, leading to ethane formation by $\cdot CH_3$ - $\cdot CH_3$ coupling.[67] **Scheme 17** illustrates this process. A previous report presenting TiO_2-graphene 2D sandwich-like nanosheets reached identical conclusions,[73] proposing again that the combination of surface mid-gap states (Ti^{3+}) and graphene layers produces a synergistic effect favoring the formation of C_2H_6.[73]

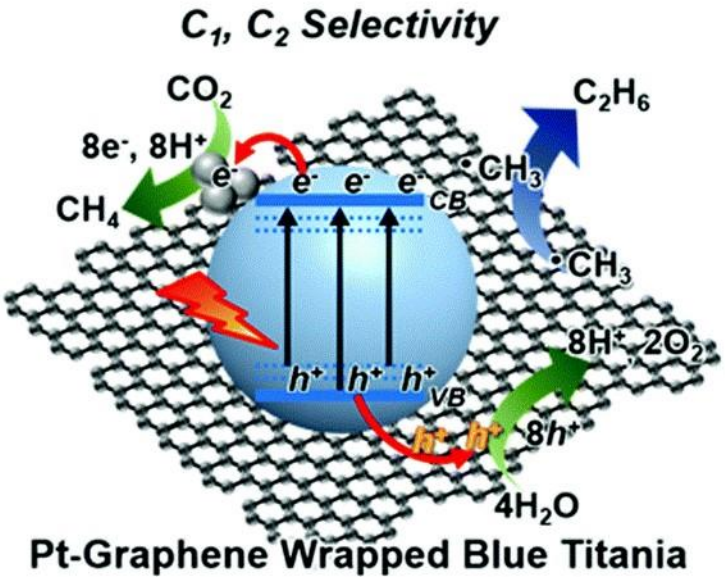

Scheme 17. Proposed mechanism for photocatalytic CO_2 reduction to CH_4 and C_2H_6 using Pt-sensitized graphene-wrapped defect-induced TiO_2 photocatalysts. Reproduced with permission.[67] Copyright (2018) Royal Society of Chemistry.

In similar approach, Ni-nanoclusters deposited on black TiO_2 demonstrated high selectivity towards CH_3CHO (10 e^- + 10 H^+) in the photocatalytic CO_2 reduction.[74] As the previously commented reduction by $NaBH_4$, TiO_2 hydrogenation promotes TiO_2 bandgap narrowing due to the generation of V_O and Ti^{3+} defetcts.[75] In the present case, Ni/black TiO_2 presents dual active sites for CO_2 adsorption and dissociation. Tauc plots obtained from diffuse reflectance UV-Vis spectroscopy measurements provided band gap values of 3.2 and 2.7 eV for TiO_2 and Ni/black TiO_2, respectively. Moreover, Ni/black TiO_2 presented mid-gap states at 0.9 eV. Theoretical calculations revealed that CO_2 simultaneously adsorbed on V_O and Ni sites should correspond to the energetically most favorable adsorption sites. According to the calculations, the double-bonded oxygen in CO_2 adsorbs to the Ti atoms near a V_O while the carbon atom is attached to the neighboring Ni atom.[74] It was also investigated, that in the absence of TiO_2 V_O sites the adsorption CO_2 mode should be different, being the CO_2 oxygen and carbon atoms adsorbed on the Ni nanocluster. In this case, experimental data shows that the product selectivity decreased, obtaining CH_3CHO and CH_3OH mixtures. Therefore, the observed selectivity towards CH_3CHO is proposed to be a consequence of the dual CO_2 adsorption giving rise to CO and O fragments on Ni and Ti(V_O) sites, respectively, during the multistep reaction process.[74] Again, this study illustrate the potential of performing theoretical calculations on valid models to rationalize selectivity changes.

In a different approach, quantum size $WO_3 \cdot 0.33H_2O$ nanotubes with large surface V_O sites have been reported to produce photocatalytic CO_2 reduction to CH_3COOH ($8e^- + 8H^+$) under solar light with 85 % selectivity.[76] The $WO_3 \cdot 0.33H_2O$ nanotubes were synthetized by oleate-assisted hydrothermal synthesis.[76] The oleate ions appear to be responsible for the formation of a high V_O concentration, since samples prepared in the absence of oleate presented much lower V_O concentration. The high V_o concentration promoted photocatalytic CO_2 reduction in aqueous $WO_3 \cdot 0.33H_2O$ nanotube dispersions to CH_3COOH, although HCOOH, CO and H_2 in trace amounts were also detected. DRIFTS studies revealed that V_O promoted CO_2 adsorption and activation, giving rise to surface bicarbonate HCO_3^- species, which in the presence of hydroxyl groups produced ·COOH intermediates leading eventually CH_3COOH formation.[76]

7. Selectivity shift through surface plasmon resonance (SPR) effect.

Considering the wide range of pathways available during the catalytic and photocatalytic CO_2 reduction, many of them having similar energy barriers and operating simultaneously in a competitive and consecutive way, a careful control of kinetic bottlenecks appears necessary for C2+ hydrocarbons production. One interesting approach carried out to promote the formation of C2+ products proposes the use of the light-induced SPR effects.[77, 78]

Hot electrons ejected as consequence of SPR excitation have been described to catalyze different organic and photoredox reactions[79] by vibrational activation of adsorbates. In one of the examples based on SPR effect to promote C2+ products in photocatalytic CO_2 reduction, Cronin et al. reported the preparation of Au NPs supported on TiO_2 exhibiting plasmonic enhancement of the photocatalytic CO_2 reduction.[80] In this study, when the Au/TiO_2 photocatalyst was irradiated

with a 532 nm laser, just at the Au plasmon band region, formation of CH_4 (8 e^- + 8 H^+) as the only product was observed. In accordance with the selective excitation of the Au plasmon, bare TiO_2 under identical excitation conditions produced negligible CH_4 amounts. It is worth noticing that the authors claimed that this activity of Au NPs is consequence of the strong electric fields generated near the Au NPs due to SPR excitation, which favor generation of e^-/h^+ pairs on the TiO_2 upon light absorption at a higher rate than it should be under normal incident light.[80] The possibility that ejected hot electrons from Au NPs become injected into TiO_2 CB was not considered, but it could be also possible considering that monochromatic 532 nm should not promote e^-/h^+ separation in pristine TiO_2. Comparison of the TiO_2 CB with the CO_2 reduction potentials to various possible products points out CH_4 as the only possible product in the present case, since other reduction potentials lie above the TiO_2 CB.[80] (**Scheme 18a**)

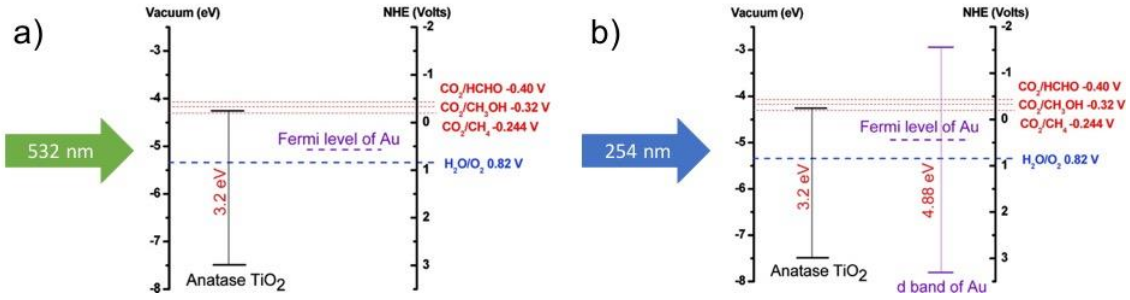

Scheme 18. Energy band alignment of TiO_2 and Au metal NPs upon 532 (a) and 254 (b) nm light excitation, and some CO_2 redox potential. Reproduced with permission.[80] Copyright (2011) American Chemical Society.

On the contrary, when the Au/TiO_2 photocatalyst was irradiated with a Hg lamp at 254 nm, C_2H_6 (14 e^- + 14 H^+), CH_2O (4 e^- + 4 H^+) and CH_3OH (6 e^- + 6 H^+) were detected, besides CH_4, in comparable amounts. In contrast, bare TiO_2 irradiation at 254 nm produced CH_4 as the only detectable product. At this high photon energy, it is likely that the products derive from the direct absorption of UV light by TiO_2 and e^- migration from the highly energetic electrons in d band of Au NPs to TiO_2[80] (**Scheme 18b**). Interestingly, the authors also reported similar product selectivity, although lower production rates, when Au NPs supported on glass were irradiated with high photon energy (254 nm), indicating that this reaction is probably taking place on the Au surface. The difference on the photocatalytic mechanism and role of Au NPs as light harvester or co-catalyst as a function of the irradiation wavelength, UV vs. visible, has also claimed in overall water splitting[81] and deserves a more detailed study as a way to control product distribution.

Moreover, the authors demonstrated that the observed behavior is not limited to Au, but the same principle can be applied to other metal NPs exhibiting SPR in the UV-Vis region. Thus, similar response under 254 nm illumination was observed for Pt and Cu metals, obtaining production rates of CH_4, C_2H_6, CH_2O and CH_3OH comparable to those obtained for Au. Therefore, it was claimed that metal NPs exhibiting SPR band can increase the selectivity towards C2+ products upon convenient excitation at appropriate wavelengths corresponding to high energy photons.[80]

The plasmonic effect on CO_2 reduction and its influence on the photocatalytic activity and selectivity was also investigated by Jain et al.[38]. They proposed colloidal Au NPs as convenient candidates for photocatalytic CO_2 reduction due to the strong cathodic polarization of excited Au NPs.[38] Thus, poly(N-vinyl-2-pyrrolidone) (PVP)-coated Au NPs of approximately 12 nm diameter were synthetized, exhibiting a SPR band centered at 520 nm. It was observed that these Au NPs

dispersed on CO_2-saturated water exhibit photocatalytic activity using isopropanol as sacrificial electron donor under monochromatic visible light irradiation (λ=488 nm, 750 mW/cm^2), yielding CH_4 (8 e^- + 8H^+) and C_2H_6 (14 e^- + 14 H^+) products. The C_2H_6 formation was investigated, providing evidence in support that it is formed from C-C coupling of C1 intermediates at the Au NP surface. Interestingly, the photocatalytic activity and selectivity was modulated not only with photon wavelength, as in the previous case, but also with the photon flux. Thus, C_2H_6 production was only observed upon irradiation with high energy photons (UV light), while CH_4 was produced at all the studied wavelengths (460-532 nm), as in the previously commented Cronin study. Interestingly, a similar trend was observed respect the photon flux. CH_4 was formed in all the investigated light intensity range (150-750 mW/cm^2), while C_2H_6 production did not take place below 300 mW/cm^2, obtaining a maximum selectivity of 40 % at 750 mW/cm^2 upon 488 nm light excitation.[38] Further experimental data suggest that high energy photons are the most suited to overcome the CO_2 activation energy to $CO_2^{\cdot-}$ species (1.9 eV). On the other hand, dimerization via C-C coupling needed a high photon flux, since MECPT processes are in kinetic competition with the ultrafast e^-/h^+ recombination rate reported for Au NPs (subpicosecond time scale).[38]

Several of the previous approaches to increase the photocatalytic activity and selectivity to C2+ hydrocarbons have been recently combined by Kuang et al.[82] using a photocatalyst based on Au-Pd alloy NPs photodeposited on TiO_2 crystals with preferential (101) facets. These facets are supposed those in which photogenerated electrons are predominantly located.[83] Upon UV-Vis light illumination formation of CH_4 (8 e^- + 8 H^+), C_2H_6 (14 e^- + 14 H^+) and C_2H_4 (12 e^- + 12 H^+) was observed, without detecting the generation of H_2. The Au-Pd alloys provided abundant active sites for CO_2 adsorption and activation. The observed photocatalytic activity and selectivity is proposed to derive from the synergistic effect of Au SPR effect to activate CO_2, together with the

well-known strong CO binding and hydrogenating activity of Pd, in combination with the preferential location of photogenerated electrons on the TiO_2 (101) facets.[82] In fact, the resultant photocatalyst showed higher activity than Au-Pd alloy NPs deposited randomly on other facets. In addition, fine tuning of the stoichiometric Au and Pd atomic ratio shows that Au_6Pd_1 exhibits the highest selectivity towards C2+ hydrocarbon, while in contrast Au_1Pd_1 forms CH_4 and CO as the only products. Further investigation of the product selectivity revealed that C2+ products are produced for Au-rich photocatalysts, indicating the ability of Au to promote the C-C coupling. However, monometallic Au sample showed a low selectivity that increases significantly upon addition of small amounts of Pd, proving the benefits of the hydrogenating function of this metal on C2+ formation. Moreover, CO intermediates can easily desorb from Au surfaces, but Pd atoms bind strongly CO resulting in the formation of C2+ products. Overall, the product selectivity in this photocatalytic systems arises from the synergistic combination of the SPR effect in Au and the strong CO adsorption and hydrogenating properties of Pd.

8. Conclusions and Outlook.

Due to the current state of the art, most of the efforts so far in photocatalytic CO_2 reduction have been aimed at increasing the efficiency of the process, in terms of higher CO_2 conversion rate. The purpose of the present review has been to stress that besides efficiency another aspect that has to be considered simultaneous in this reaction is product selectivity. Due to their higher added value, formation of C2+ products can be of larger interest than methane, carbon monoxide and formate that are the typical major products in most of the reports. When formed, the amounts of C2+ is typically low, the record being about 40 % of combined percentages, there being of

interest in increasing their proportion and selectivity. The current knowledge is empirical and based on the experimental results with a poor rationalization of the factors that control formation of C2+ products. From the present data, it seems that every factor that increases accumulation of charge carriers and protons favor the formation of C2+ products. The present review has grouped the existing reports describing C2+ products according to the various factor that influence the formation of C2+, like photocatalyst structuring, adequate co-catalysts, operation of SPR effects and defects, among other possible parameters. A summary of the most relevant catalysts, products and reaction conditions is presented a Table 2. Moreover, the suppression of the H_2 evolution reaction, which consumes e^- and H^+ could strongly influence not only the reaction yield, but also their selectivity towards multi-carbon products. Further strategies to inhibit this lateral reaction must be considered in order to improve both reaction yield and C2+ selectivity. In a similar way, the use of continuous flow systems would benefit not only the implementation of this technology to the industrial scale, but also it can influence the product selectivity by means of the release of weakly bind intermediates and products from the catalysts surface, avoiding their re-oxidation in the photocatalysts surface.

It can be expected that this area will receive intensive research effort in the near years with the aim of gaining selectivity in the photocatalytic CO_2 conversion to valuable products like alcohols, alkenes and aromatic hydrocarbons, rather than focus exclusively on methane or CO that are of much less commercial value.

Table 2. Summary of the most relevant photocatalysts reported in this review indicating their product selectivity and reaction conditions.

Photocatalysts	C2+ selectivity	Reaction conditions	Ref.

MWCNTs/TiO_2(anatase)	69.7 % CH_3CH_2OH	H_2O:CO_2, 5:1 (mol:mol), 15 W UV lamp@365 nm, 5 h	[46]
LHCII/Rh:P25 TiO_2	78.4 % CH_3CHO+ 5.9 % CH_3OCHO	Aqueous dispersion CO_2 saturated , Xe lamp @362 mW/cm^2, 6h.	[48]
15 wt% Cu/GO	100 % CH_3CHO	Moisted CO_2, halogen lamp @100 mW/cm^2, 2h.	[50]
200 oriented Cu_2O/G	100% CH_3CH_2OH	Operated under liquid-phase continuous flow, 28.3 mW/cm^2 lamp @ 254 nm.	[12]
Pt/TaON	89.5 % CH_3CH_2OH + 10.5 % CH_3CHO	$NaHCO_3$ aqueous solution CO_2 saturated, 1002 W/m^2 ($\lambda > 420$ nm)	[51]
PtCu/TiO_2 NTs	14.3 % C_2H_6 + 7.1 % C_2H_4	CO_2 (0.998% in N_2) flow through H_2O, 100 mW/cm^2	[55]
CoFeAl-LDH	35 % C2+	CO_2/ H_2 /Ar=15/60/25; 0.18 MPa;, 300 W Xe lamp irradiation 2h.	[56]
Nafion/Pd-TiO_2	6.4 % C_2H_6	$NaHCO_3$ aqueous dispersion CO_2 saturated, 300 W Xe lamp ($\lambda >$ 300 nm), 5h	[57]
CdS/Cu-TNTs	31.1% C_2H_6 + 17.9 % C_3H_8 +1.3 % C_3H_6 + 0.5 % C_2H_4	Aqueous dispersion CO_2 saturated, 450 W Xe lamp ($\lambda >$ 420 nm), 5h	[58]
Na/Co@C	39.5 % C_xH_y (C2-C6) + 6. 5% CH_3CH_2OH	CO_2/N_2/H_2 = 20/20/100 (2.8 bar), 1000 W Xe lamp 24 kW/cm^2	[62]
Pt-G/defect-induced TiO_2	30 % C_2H_6	Moisted CO_2, 100 W solar simulator 100 mW/cm^2.	[67]
Ni/$TiO_{2[Vo]}$	100% CH_3CHO	Moisted CO_2, 300 W halogen lamp	[74]
$WO_3 \cdot 0.33H_2O$	85% CH_3COOH	Aqueous dispersion CO_2 saturated, 100 mW/cm^2 sun-siulated light, 10h	[76]
Au/TiO_2	27 % C_2H_6	Moisted CO_2, Hg lamp @ 254 nm, 20mW/cm^2	[79]
Au NPs	100 % C_2H_6	Moisted CO_2 using isopropanol as sacrificial, ($\lambda >$ 488 nm, 750 mW/cm^2)	[38]
AuPd/(101) TiO_2	4 % C_2H_6 + 4 % C_2H_4	$NaHCO_3$ aqueous dispersion CO_2 saturated, 300 W Xe lamp	[82]

AUTHOR INFORMATION

Corresponding Author

* E-mail: hgarcia@qim.upv.es

Tel: +34 963877807

Author Contributions

J.A. and Y.P. wrote part of the manuscript. H. G. supervised the research and wrote most of the manuscript. All the authors discussed the results and corrected the article draft.

Funding Sources

Financial support by the Spanish Ministry of Science and Innovation (Severo Ochoa and CTQ2018-89237-CO2-R1) and Generalitat Valenciana (Prometeo 2017/83) is gratefully acknowledged.

ACKNOWLEDGMENT

Yong Peng also thanks the Universitat Politècnica de València for a predoctoral scholarship.

REFERENCES

1. Low, J.; Cheng, B.; Yu, J., Surface modification and enhanced photocatalytic CO2 reduction performance of TiO2: a review. *Applied Surface Science* **2017,** *392*, 658-686.
2. Zeng, S.; Kar, P.; Thakur, U. K.; Shankar, K., A review on photocatalytic CO2 reduction using perovskite oxide nanomaterials. *Nanotechnology* **2018,** *29* (5), 052001.
3. Ola, O.; Maroto-Valer, M. M., Review of material design and reactor engineering on TiO2 photocatalysis for CO2 reduction. *Journal of Photochemistry and Photobiology C: Photochemistry Reviews* **2015,** *24*, 16-42.

4. Tachibana, Y.; Vayssieres, L.; Durrant, J. R., Artificial photosynthesis for solar water-splitting. *Nature Photonics* **2012,** *6* (8), 511.
5. Gust, D.; Moore, T. A.; Moore, A. L., Solar fuels via artificial photosynthesis. *Accounts of chemical research* **2009,** *42* (12), 1890-1898.
6. Zhang, T.; Lin, W., Metal–organic frameworks for artificial photosynthesis and photocatalysis. *Chemical Society Reviews* **2014,** *43* (16), 5982-5993.
7. Hao, Y.; Steinfeld, A., Fuels from water, CO2 and solar energy. *Science Bulletin* **2017,** *62* (16), 1099-1101.
8. Saeidi, S.; Amin, N. A. S.; Rahimpour, M. R., Hydrogenation of CO2 to value-added products—A review and potential future developments. *Journal of CO2 utilization* **2014,** *5*, 66-81.
9. Ma, J.; Sun, N.; Zhang, X.; Zhao, N.; Xiao, F.; Wei, W.; Sun, Y., A short review of catalysis for CO2 conversion. *Catalysis Today* **2009,** *148* (3-4), 221-231.
10. Huang, C.-H.; Tan, C.-S., A review: CO2 utilization. *Aerosol Air Qual. Res* **2014,** *14* (2), 480-499.
11. Jia, J.; Wang, H.; Lu, Z.; O'Brien, P. G.; Ghoussoub, M.; Duchesne, P.; Zheng, Z.; Li, P.; Qiao, Q.; Wang, L., Photothermal catalyst engineering: hydrogenation of gaseous CO2 with high activity and tailored selectivity. *Advanced Science* **2017,** *4* (10), 1700252.
12. Hurtado, L.; Natividad, R.; García, H., Photocatalytic activity of Cu2O supported on multi layers graphene for CO2 reduction by water under batch and continuous flow. *Catalysis Communications* **2016,** *84*, 30-35.
13. Wu, J.; Huang, Y.; Ye, W.; Li, Y., CO2 Reduction: From the Electrochemical to Photochemical Approach. *Advanced Science* **2017,** *4* (11), 1700194.
14. Seo, H.; Katcher, M. H.; Jamison, T. F., Photoredox activation of carbon dioxide for amino acid synthesis in continuous flow. *Nature Chemistry* **2017,** *9* (5), 453-456.
15. Vu, N.-N.; Kaliaguine, S.; Do, T.-O., Critical Aspects and Recent Advances in Structural Engineering of Photocatalysts for Sunlight-Driven Photocatalytic Reduction of CO2 into Fuels. *Advanced Functional Materials* **2019,** *29* (31), 1901825.
16. Niu, J.; Shen, S.; Zhou, L.; Liu, Z.; Feng, P.; Ou, X.; Qiang, Y., Synthesis and hydrogenation of anatase TiO2 microspheres composed of porous single crystals for significantly improved photocatalytic activity. *RSC Advances* **2016,** *6* (67), 62907-62910.
17. Neaţu, Ş.; Maciá-Agulló, J. A.; Concepción, P.; Garcia, H., Gold–Copper Nanoalloys Supported on TiO2 as Photocatalysts for CO2 Reduction by Water. *Journal of the American Chemical Society* **2014,** *136* (45), 15969-15976.
18. Xiong, Z.; Lei, Z.; Kuang, C.-C.; Chen, X.; Gong, B.; Zhao, Y.; Zhang, J.; Zheng, C.; Wu, J. C. S., Selective photocatalytic reduction of CO2 into CH4 over Pt-Cu2O TiO2 nanocrystals: The interaction between Pt and Cu2O cocatalysts. *Applied Catalysis B: Environmental* **2017,** *202*, 695-703.
19. Zhai, Q.; Xie, S.; Fan, W.; Zhang, Q.; Wang, Y.; Deng, W.; Wang, Y., Photocatalytic Conversion of Carbon Dioxide with Water into Methane: Platinum and Copper(I) Oxide Co-catalysts with a Core–Shell Structure. *Angewandte Chemie International Edition* **2013,** *52* (22), 5776-5779.
20. Wei, W.; Jinlong, G., Methanation of carbon dioxide: an overview. *Frontiers of Chemical Science and Engineering* **2011,** *5* (1), 2-10.
21. Frontera, P.; Macario, A.; Ferraro, M.; Antonucci, P., Supported Catalysys for CO2 Methanation: A review. *Catalysts* **2017,** *7*, 59.

22. Mateo, D.; Albero, J.; García, H., Graphene supported NiO/Ni nanoparticles as efficient photocatalyst for gas phase CO2 reduction with hydrogen. *Applied Catalysis B: Environmental* **2018,** *224*, 563-571.
23. Zhao, J.; Yang, Q.; Shi, R.; Waterhouse, G. I. N.; Zhang, X.; Wu, L.-Z.; Tung, C.-H.; Zhang, T., FeO–CeO2 nanocomposites: an efficient and highly selective catalyst system for photothermal CO2 reduction to CO. *NPG Asia Materials* **2020,** *12* (1), 5.
24. Xiao, J.-D.; Jiang, H.-L., Metal–Organic Frameworks for Photocatalysis and Photothermal Catalysis. *Accounts of Chemical Research* **2019,** *52* (2), 356-366.
25. Wang, C.; Sun, Z.; Zheng, Y.; Hu, Y. H., Recent progress in visible light photocatalytic conversion of carbon dioxide. *Journal of Materials Chemistry A* **2019,** *7* (3), 865-887.
26. Voiry, D.; Shin, H. S.; Loh, K. P.; Chhowalla, M., Low-dimensional catalysts for hydrogen evolution and CO2 reduction. *Nature Reviews Chemistry* **2018,** *2* (1), 0105.
27. Lee, Y. Y.; Jung, H. S.; Kang, Y. T., A review: Effect of nanostructures on photocatalytic CO2 conversion over metal oxides and compound semiconductors. *Journal of CO2 Utilization* **2017,** *20*, 163-177.
28. Yang, M.-Q.; Xu, Y.-J., Photocatalytic conversion of CO2 over graphene-based composites: current status and future perspective. *Nanoscale Horizons* **2016,** *1* (3), 185-200.
29. Peng, C.; Reid, G.; Wang, H.; Hu, P., Perspective: Photocatalytic reduction of CO2 to solar fuels over semiconductors. *The Journal of Chemical Physics* **2017,** *147* (3), 030901.
30. Lei, Z.; Xue, Y.; Chen, W.; Qiu, W.; Zhang, Y.; Horike, S.; Tang, L., MOFs-Based Heterogeneous Catalysts: New Opportunities for Energy-Related CO2 Conversion. *Advanced Energy Materials* **2018,** *8* (32), 1801587.
31. Sun, Z.; Talreja, N.; Tao, H.; Texter, J.; Muhler, M.; Strunk, J.; Chen, J., Catalysis of Carbon Dioxide Photoreduction on Nanosheets: Fundamentals and Challenges. *Angewandte Chemie International Edition* **2018,** *57* (26), 7610-7627.
32. Chen, G.; Waterhouse, G. I. N.; Shi, R.; Zhao, J.; Li, Z.; Wu, L.-Z.; Tung, C.-H.; Zhang, T., From Solar Energy to Fuels: Recent Advances in Light-Driven C1 Chemistry. *Angewandte Chemie International Edition* **2019,** *58* (49), 17528-17551.
33. U.S Energy Information Administration. https://www.eia.gov/.
34. Jouny, M.; Luc, W.; Jiao, F., General Techno-Economic Analysis of CO2 Electrolysis Systems. *Industrial & Engineering Chemistry Research* **2018,** *57* (6), 2165-2177.
35. Kibria, M. G.; Edwards, J. P.; Gabardo, C. M.; Dinh, C.-T.; Seifitokaldani, A.; Sinton, D.; Sargent, E. H., Electrochemical CO2 Reduction into Chemical Feedstocks: From Mechanistic Electrocatalysis Models to System Design. *Advanced Materials* **2019,** *31* (31), 1807166.
36. Fu, J.; Jiang, K.; Qiu, X.; Yu, J.; Liu, M., Product selectivity of photocatalytic CO2 reduction reactions. *Materials Today* **2019,** *32*, 222-243.
37. Habisreutinger, S. N.; Schmidt-Mende, L.; Stolarczyk, J. K., Photocatalytic Reduction of CO2 on TiO2 and Other Semiconductors. *Angewandte Chemie International Edition* **2013,** *52* (29), 7372-7408.
38. Yu, S.; Wilson, A. J.; Heo, J.; Jain, P. K., Plasmonic Control of Multi-Electron Transfer and C–C Coupling in Visible-Light-Driven CO2 Reduction on Au Nanoparticles. *Nano Letters* **2018,** *18* (4), 2189-2194.
39. Unruh, D.; Pabst, K.; Schaub, G., Fischer−Tropsch Synfuels from Biomass: Maximizing Carbon Efficiency and Hydrocarbon Yield. *Energy & Fuels* **2010,** *24* (4), 2634-2641.

40. Klerk, A. l., Fischer–Tropsch Synthesis. In *Fischer-Tropsch Refining*, Klerk, A. d., Ed. 2011; pp 73-103.
41. Jager, B., Developments in Fischer-Tropsch technology. In *Studies in Surface Science and Catalysis*, Parmaliana, A.; Sanfilippo, D.; Frusteri, F.; Vaccari, A.; Arena, F., Eds. Elsevier: 1998; Vol. 119, pp 25-34.
42. Gu, B.; Khodakov, A. Y.; Ordomsky, V. V., Selectivity shift from paraffins to α-olefins in low temperature Fischer–Tropsch synthesis in the presence of carboxylic acids. *Chemical Communications* **2018,** *54* (19), 2345-2348.
43. Brady, R. C.; Pettit, R., Mechanism of the Fischer-Tropsch reaction. The chain propagation step. *Journal of the American Chemical Society* **1981,** *103* (5), 1287-1289.
44. Zhang, Q.; Deng, W.; Wang, Y., Recent advances in understanding the key catalyst factors for Fischer-Tropsch synthesis. *Journal of Energy Chemistry* **2013,** *22* (1), 27-38.
45. Jahangiri, H.; Bennett, J.; Mahjoubi, P.; Wilson, K.; Gu, S., A review of advanced catalyst development for Fischer–Tropsch synthesis of hydrocarbons from biomass derived syn-gas. *Catalysis Science & Technology* **2014,** *4* (8), 2210-2229.
46. Xia, X.-H.; Jia, Z.-J.; Yu, Y.; Liang, Y.; Wang, Z.; Ma, L.-L., Preparation of multi-walled carbon nanotube supported TiO2 and its photocatalytic activity in the reduction of CO2 with H2O. *Carbon* **2007,** *45* (4), 717-721.
47. Yue, W.; Randorn, C.; Attidekou, P. S.; Su, Z.; Irvine, J. T. S.; Zhou, W., Syntheses, Li Insertion, and Photoactivity of Mesoporous Crystalline TiO2. *Advanced Functional Materials* **2009,** *19* (17), 2826-2833.
48. Lee, C.-W.; Antoniou Kourounioti, R.; Wu, J. C. S.; Murchie, E.; Maroto-Valer, M.; Jensen, O. E.; Huang, C.-W.; Ruban, A., Photocatalytic conversion of CO2 to hydrocarbons by light-harvesting complex assisted Rh-doped TiO2 photocatalyst. *Journal of CO2 Utilization* **2014,** *5*, 33-40.
49. Blankenship, R. E., *Molecular Mechanims of Photosynthesis, 2nd Edition*. Wiley Blackwell: 2002; Vol. 7, p d765-d783.
50. Shown, I.; Hsu, H.-C.; Chang, Y.-C.; Lin, C.-H.; Roy, P. K.; Ganguly, A.; Wang, C.-H.; Chang, J.-K.; Wu, C.-I.; Chen, L.-C.; Chen, K.-H., Highly Efficient Visible Light Photocatalytic Reduction of CO2 to Hydrocarbon Fuels by Cu-Nanoparticle Decorated Graphene Oxide. *Nano Letters* **2014,** *14* (11), 6097-6103.
51. Han, Q.; Zhou, Y.; Tang, L.; Li, P.; Tu, W.; Li, L.; Li, H.; Zou, Z., Synthesis of single-crystalline, porous TaON microspheres toward visible-light photocatalytic conversion of CO2 into liquid hydrocarbon fuels. *RSC Advances* **2016,** *6* (93), 90792-90796.
52. Ran, J.; Jaroniec, M.; Qiao, S.-Z., Cocatalysts in Semiconductor-based Photocatalytic CO2 Reduction: Achievements, Challenges, and Opportunities. *Advanced Materials* **2018,** *30* (7), 1704649.
53. Ran, J.; Zhang, J.; Yu, J.; Jaroniec, M.; Qiao, S. Z., Earth-abundant cocatalysts for semiconductor-based photocatalytic water splitting. *Chemical Society Reviews* **2014,** *43* (22), 7787-7812.
54. Varghese, O. K.; Paulose, M.; LaTempa, T. J.; Grimes, C. A., High-Rate Solar Photocatalytic Conversion of CO2 and Water Vapor to Hydrocarbon Fuels. *Nano Letters* **2009,** *9* (2), 731-737.
55. Zhang, X.; Han, F.; Shi, B.; Farsinezhad, S.; Dechaine, G. P.; Shankar, K., Photocatalytic Conversion of Diluted CO2 into Light Hydrocarbons Using Periodically

Modulated Multiwalled Nanotube Arrays. *Angewandte Chemie International Edition* **2012,** *51* (51), 12732-12735.
56. Chen, G.; Gao, R.; Zhao, Y.; Li, Z.; Waterhouse, G. I. N.; Shi, R.; Zhao, J.; Zhang, M.; Shang, L.; Sheng, G.; Zhang, X.; Wen, X.; Wu, L.-Z.; Tung, C.-H.; Zhang, T., Alumina-Supported CoFe Alloy Catalysts Derived from Layered-Double-Hydroxide Nanosheets for Efficient Photothermal CO2 Hydrogenation to Hydrocarbons. *Advanced Materials* **2018,** *30* (3), 1704663.
57. Kim, W.; Seok, T.; Choi, W., Nafion layer-enhanced photosynthetic conversion of CO2 into hydrocarbons on TiO2 nanoparticles. *Energy & Environmental Science* **2012,** *5* (3), 6066-6070.
58. Park, H.; Ou, H.-H.; Colussi, A. J.; Hoffmann, M. R., Artificial Photosynthesis of C1–C3 Hydrocarbons from Water and CO2 on Titanate Nanotubes Decorated with Nanoparticle Elemental Copper and CdS Quantum Dots. *The Journal of Physical Chemistry A* **2015,** *119* (19), 4658-4666.
59. Du, H.; Williams, C. T.; Ebner, A. D.; Ritter, J. A., In Situ FTIR Spectroscopic Analysis of Carbonate Transformations during Adsorption and Desorption of CO2 in K-Promoted HTlc. *Chemistry of Materials* **2010,** *22* (11), 3519-3526.
60. Panagiotopoulou, P.; Kondarides, D. I., Effects of alkali promotion of TiO2 on the chemisorptive properties and water–gas shift activity of supported noble metal catalysts. *Journal of Catalysis* **2009,** *267* (1), 57-66.
61. Hölzl J.; F.K., S., *Work function of metals*. Springer Berlin, 1979; Vol. 85, p 1-150.
62. Liu, L.; Puga, A. V.; Cored, J.; Concepción, P.; Pérez-Dieste, V.; García, H.; Corma, A., Sunlight-assisted hydrogenation of CO2 into ethanol and C2+ hydrocarbons by sodium-promoted Co@C nanocomposites. *Applied Catalysis B: Environmental* **2018,** *235*, 186-196.
63. D'Arienzo, M.; Carbajo, J.; Bahamonde, A.; Crippa, M.; Polizzi, S.; Scotti, R.; Wahba, L.; Morazzoni, F., Photogenerated defects in shape-controlled TiO2 anatase nanocrystals: a probe to evaluate the role of crystal facets in photocatalytic processes. *Journal of the American Chemical Society* **2011,** *133* (44), 17652-17661.
64. Kong, M.; Li, Y.; Chen, X.; Tian, T.; Fang, P.; Zheng, F.; Zhao, X., Tuning the relative concentration ratio of bulk defects to surface defects in TiO2 nanocrystals leads to high photocatalytic efficiency. *Journal of the American Chemical Society* **2011,** *133* (41), 16414-16417.
65. Nowotny, M. K.; Sheppard, L. R.; Bak, T.; Nowotny, J., Defect chemistry of titanium dioxide. Application of defect engineering in processing of TiO2-based photocatalysts. *The Journal of Physical Chemistry C* **2008,** *112* (14), 5275-5300.
66. Bai, S.; Zhang, N.; Gao, C.; Xiong, Y., Defect engineering in photocatalytic materials. *Nano Energy* **2018,** *53*, 296-336.
67. Sorcar, S.; Thompson, J.; Hwang, Y.; Park, Y. H.; Majima, T.; Grimes, C. A.; Durrant, J. R.; In, S.-I., High-rate solar-light photoconversion of CO2 to fuel: controllable transformation from C1 to C2 products. *Energy & Environmental Science* **2018,** *11* (11), 3183-3193.
68. Sorescu, D. C.; Al-Saidi, W. A.; Jordan, K. D., CO2 adsorption on TiO2(101) anatase: A dispersion-corrected density functional theory study. *The Journal of Chemical Physics* **2011,** *135* (12), 124701.

69. Yin, W.-J.; Wen, B.; Bandaru, S.; Krack, M.; Lau, M. W.; Liu, L.-M., The Effect of Excess Electron and hole on CO2 Adsorption and Activation on Rutile (110) surface. *Scientific Reports* **2016,** *6* (1), 23298.
70. Deskins, N. A.; Rousseau, R.; Dupuis, M., Defining the Role of Excess Electrons in the Surface Chemistry of TiO2. *The Journal of Physical Chemistry C* **2010,** *114* (13), 5891-5897.
71. Razzaq, A.; Sinhamahapatra, A.; Kang, T.-H.; Grimes, C. A.; Yu, J.-S.; In, S.-I., Efficient solar light photoreduction of CO2 to hydrocarbon fuels via magnesiothermally reduced TiO2 photocatalyst. *Applied Catalysis B: Environmental* **2017,** *215*, 28-35.
72. Liu, J.; Bai, H.; Wang, Y.; Liu, Z.; Zhang, X.; Sun, D. D., Self-Assembling TiO2 Nanorods on Large Graphene Oxide Sheets at a Two-Phase Interface and Their Anti-Recombination in Photocatalytic Applications. *Advanced Functional Materials* **2010,** *20* (23), 4175-4181.
73. Tu, W.; Zhou, Y.; Liu, Q.; Yan, S.; Bao, S.; Wang, X.; Xiao, M.; Zou, Z., An In Situ Simultaneous Reduction-Hydrolysis Technique for Fabrication of TiO2-Graphene 2D Sandwich-Like Hybrid Nanosheets: Graphene-Promoted Selectivity of Photocatalytic-Driven Hydrogenation and Coupling of CO2 into Methane and Ethane. *Advanced Functional Materials* **2013,** *23* (14), 1743-1749.
74. Billo, T.; Fu, F.-Y.; Raghunath, P.; Shown, I.; Chen, W.-F.; Lien, H.-T.; Shen, T.-H.; Lee, J.-F.; Chan, T.-S.; Huang, K.-Y.; Wu, C.-I.; Lin, M. C.; Hwang, J.-S.; Lee, C.-H.; Chen, L.-C.; Chen, K.-H., Ni-Nanocluster Modified Black TiO2 with Dual Active Sites for Selective Photocatalytic CO2 Reduction. *Small* **2018,** *14* (2), 1702928.
75. Chen, X.; Liu, L.; Yu, P. Y.; Mao, S. S., Increasing Solar Absorption for Photocatalysis with Black Hydrogenated Titanium Dioxide Nanocrystals. *Science* **2011,** *331* (6018), 746.
76. Sun, S.; Watanabe, M.; Wu, J.; An, Q.; Ishihara, T., Ultrathin WO3·0.33H2O Nanotubes for CO2 Photoreduction to Acetate with High Selectivity. *Journal of the American Chemical Society* **2018,** *140* (20), 6474-6482.
77. Hou, W.; Cronin, S. B., A review of surface plasmon resonance-enhanced photocatalysis. *Advanced Functional Materials* **2013,** *23* (13), 1612-1619.
78. Zhang, X.; Chen, Y. L.; Liu, R.-S.; Tsai, D. P., Plasmonic photocatalysis. *Reports on Progress in Physics* **2013,** *76* (4), 046401.
79. Gellé, A.; Jin, T.; de la Garza, L.; Price, G. D.; Besteiro, L. V.; Moores, A., Applications of Plasmon-Enhanced Nanocatalysis to Organic Transformations. *Chemical Reviews* **2020,** *120* (2), 986-1041.
80. Hou, W.; Hung, W. H.; Pavaskar, P.; Goeppert, A.; Aykol, M.; Cronin, S. B., Photocatalytic Conversion of CO2 to Hydrocarbon Fuels via Plasmon-Enhanced Absorption and Metallic Interband Transitions. *ACS Catalysis* **2011,** *1* (8), 929-936.
81. Montes-Navajas, P.; Serra, M.; Garcia, H., Influence of the irradiation wavelength on the photocatalytic activity of Au–Pt nanoalloys supported on TiO 2 for hydrogen generation from water. *Catalysis Science & Technology* **2013,** *3* (9), 2252-2258.
82. Chen, Q.; Chen, X.; Fang, M.; Chen, J.; Li, Y.; Xie, Z.; Kuang, Q.; Zheng, L., Photo-induced Au–Pd alloying at TiO2 {101} facets enables robust CO2 photocatalytic reduction into hydrocarbon fuels. *Journal of Materials Chemistry A* **2019,** *7* (3), 1334-1340.
83. Liu, C.; Han, X.; Xie, S.; Kuang, Q.; Wang, X.; Jin, M.; Xie, Z.; Zheng, L., Enhancing the Photocatalytic Activity of Anatase TiO2 by Improving the Specific Facet-Induced Spontaneous Separation of Photogenerated Electrons and Holes. *Chemistry–An Asian Journal* **2013,** *8* (1), 282-289.